water

MDPI

*Review*

# Diatom Biosilica: A Useful Natural Material for Biomedical Engineering

**Daehyeon Yoo [1], Minyoung Lee [1], Yoseph Seo [1], Jinwook Yoon [1], Eunseok Jang [1], Gaeun Lee [1], Daeryul Kwon [2], Sang Deuk Lee [2], Junhong Min [3,*] and Taek Lee [1,*]**

[1] Department of Chemical Engineering, Kwangwoon University, 20 Kwangwoon-Ro, Nowon-Gu, Seoul 01897, Republic of Korea; lovydh@kw.ac.kr (D.Y.); dalsdud005@kw.ac.kr (M.L.); akdldytpq12@kw.ac.kr (Y.S.); yjwkk@kw.ac.kr (J.Y.); bluedip28@kw.ac.kr (E.J.); garlic36@kw.ac.kr (G.L.)
[2] Protist Research Division, Biological Resources Research Department, Nakdonggang National Institute of Biological Resources (NNIBR), 137, Donam 2-gil, Sangju-si 37242, Republic of Korea; kdyrevive@nnibr.re.kr (D.K.); diatom83@nnibr.re.kr (S.D.L.)
[3] School of Integrative Engineering, Chung-Ang University, Heukseok-dong, Dongjak-gu, Seoul 06974, Republic of Korea
* Correspondence: junmin@cau.ac.kr (J.M.); tlee@kw.ac.kr (T.L.)

## Abstract

Silica-based materials are recognized as effective functional materials across diverse industrial fields, including biomedicine (e.g., drug delivery systems (DDS), biosensors, and tissue engineering), owing to their excellent stability and physicochemical characteristics. Among them, diatom biosilica (DB), which constitutes a major part of aquatic biomass, recently gained significant attention as a valuable biomaterial following breakthroughs in its innovative surface structure, superior biocompatibility and multifunctionality. Therefore, DB is emerging as an alternative to synthetic materials used in the biomedical field. This review comprehensively examines the diverse biological properties of DB, followed by an analysis of harvesting and purification strategies. Then, the current application status of DB in two principal biomedical domains, DDS and biosensors, is evaluated. Furthermore, the convergence of these domains into theragnostic applications addresses a significant unmet clinical need for simultaneous therapeutic intervention and diagnostic monitoring, positioning DB as a transformative biomaterial solution. The unique combination of natural hierarchical architecture, tunable surface properties, and excellent biocompatibility make DB promising candidates for next-generation integrated biomedical platforms to address the growing demand of personalized medicine and precision healthcare solutions.

**Keywords:** diatom biosilica; biomaterials; drug delivery systems; biosensors; theragnosis

check for updates

Academic Editor: Laura Bulgariu

Received: 27 June 2025
Revised: 28 July 2025
Accepted: 31 July 2025
Published: 11 August 2025

**Citation:** Yoo, D.; Lee, M.; Seo, Y.; Yoon, J.; Jang, E.; Lee, G.; Kwon, D.; Lee, S.D.; Min, J.; Lee, T. Diatom Biosilica: A Useful Natural Material for Biomedical Engineering. *Water* **2025**, *17*, 2373. https://doi.org/10.3390/w17162373

**Copyright:** © 2025 by the authors. Licensee MDPI, Basel, Switzerland. This article is an open access article distributed under the terms and conditions of the Creative Commons Attribution (CC BY) license (https://creativecommons.org/licenses/by/4.0/).

## 1. Introduction

Biomass-based natural resources are becoming a key strategy in sustainable biomaterial development. Their functionality and biocompatibility are being re-evaluated, expanding their potential as high-value biomaterials [1]. This superior biocompatibility, compared to synthetic alternatives, offers a paradigm shift toward environmentally sustainable technological approaches [2]. Microalgal biomass serves as a sustainable source of alternative products to synthetic materials, including biodiesel and bioplastics, as well as high-value compounds such as animal and aquaculture feed, essential fatty acids (e.g., Omega-3), pigments (e.g., chlorophylls), and pharmaceuticals [3–5]. Among these resources, diatom biosilica (DB), with its three-dimensional porous architecture, has gained significant attention as a high-performance inorganic-based biomaterial in the biomedical field [6,7].

Unlike other microalgae, whose cell walls are typically composed of polysaccharides and glycoproteins, diatoms have silica cell walls composed of $SiO_2$ [8]. This natural silica cell wall provides strong resistance to various physical/chemical environments [9]. In addition, the nanoscale porous hierarchical structures evenly distributed on their surfaces exhibit excellent hygroscopicity and solubility for insoluble substances, facilitating complex material exchange with the outer environment [10,11]. Because of these characteristics, DB is currently used as a biomaterial for various medical purposes [12].

The elaborate porous structure and surface functionality of DB materials render them suitable for the biomedical field [13]. Based on this, DB materials are being applied in the development of sustained-release formulations in the drug delivery system (DDS) field [14]. Drugs can be easily loaded into DB matrices through internal encapsulation and external adsorption [15,16], demonstrating superior sustained-release kinetics compared to conventional free drugs *via* the enhanced solubilization of hydrophobic pharmaceuticals [14]. In biosensing, DB is used as a pretreatment material in the form of a filter based on its surface, which is easy to modify and has excellent hygroscopicity, or as a material to improve the performance of optical sensors based on the optical properties derived from the porous structure of silica [17]. Therefore, these properties of DB suggest its potential as an excellent biomaterial for theragnosis, in which the two biomedical fields are integrated.

Despite extensive investigations into the potential of DB for biomaterials, systematic reviews addressing essential preprocessing methodologies, including harvesting and purification protocols for biomedical implementation, remain insufficient. Therefore, the present study emphasizes the necessity of understanding the biological properties of DB and cultivation–purification strategies that constitute fundamental prerequisites for biomedical utilization. It also discusses how the advantages of DB as a survival tool used by diatoms to adapt to the environment can provide inspiration for excellent biomaterials. Through a systematic comparative analysis, we provide a comprehensive assessment of DB as a versatile biomaterial for theragnostic platforms, which seamlessly integrate DDS and biosensing functionalities, thereby offering considerable promise for next-generation therapeutic interventions. Collectively, this review establishes a conceptual and practical framework for understanding the structure–function relationship of DB and its strategic advantages in the advancement of cutting-edge biomedical technologies.

## 2. Biological Properties of DB and Its Biofabrication

DB is formed by enzyme-based silicon-fixing and biosynthetic processes and functions as an environmental adaptation strategy for diatoms [18]. DB plays a diverse biological function, such as UV protection, defense against predators, light-scattering control, and carbon and nutrient absorption. Its functionality extends beyond simple support and has a profound effect on the survival and environmental adaptation of diatoms [19–21]. Purified DB is considered an excellent biomaterial in the biomedical field, such as in DDS and biosensing, owing to its unique properties, such as its large surface area, excellent mechanical strength, thermal stability, and uniform microporous structure [9,22]. In this section, we describe in detail the functionality of DB, which can be considered as a highly functional natural biomaterial, and the methods used to obtain it.

### *2.1. DB Biosynthesis*

DB synthesis is closely associated with the cell cycle of diatoms, during which a complex and hierarchical silica shell is formed *via* a biosynthetic process involving Si metabolism [23,24]. The primary organelles responsible for the formation of the silica cell wall are silica deposition vesicles (SDV) that concentrate silica precursors (mainly orthosilicic acid) and are absorbed from the external environment into the cytoplasm [25].

Concentrated silica is then polymerized into the porous hierarchical structure of DB through the involvement of various enzymes related to silica metabolism, such as silaffins and silicanin-1 (Sin1) [26]. This sophisticated biosynthetic machinery suggests that diatoms have evolved highly refined mechanisms for creating precisely engineered silica structures, which may hold significant implications for biomimetic material design.

The potential for harnessing these natural biosynthetic pathways becomes particularly evident when examining the genetic basis of DB formation. Molecular biology studies on DB synthesis in diatoms have reported that the morphology and mechanical strength of DB are influenced considerably by genetic factors [27]. According to Görlich et al. [28], Sin1, a diatom membrane protein, plays an important role in DB formation in *Thalassiosira pseudonana*. This research team generated a knockout mutant lacking Sin1 (through genetic manipulation) and observed the morphological changes and mechanical properties of wild-type and mutant DB. While the wild-type DB showed a normal arrangement of silica costae that extended radially from the center of the valve and branched toward the periphery (Figure 1a), the mutant-type DB exhibited considerable cross-linking loss (Figure 1b–d). Subsequently, the mechanical strength of DB was evaluated based on displacement-controlled tests using a diamond tip with a penetration depth of 1 µm. The results showed that the wild-type DB completely returned to their initial shapes after contraction (Figure 1e–g), whereas the mutant valves exhibited a buckled shape (Figure 1h–j). This indicates that the Sin1 present in the SDV membrane is essential for DB formation and is a key factor in characterizing morphological aberrations and mechanical strength. Genetic control over DB biosynthesis enables tunability for biomedical material design, offering unprecedented opportunities for engineering DB properties to meet specific application requirements in therapeutic and diagnostic systems.

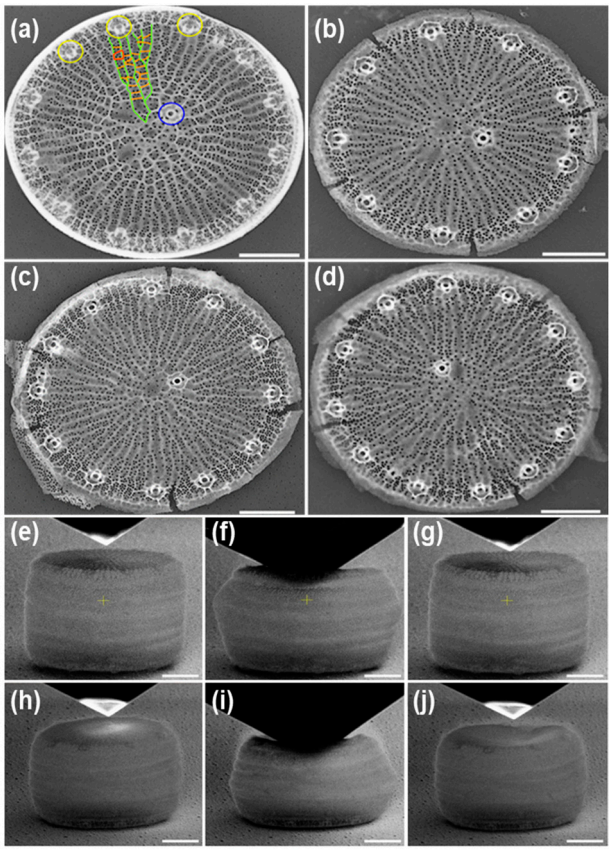



**Figure 1.** Comparison of biosilica morphology. Representative TEM images of *T. pseudonana* valve biosilica from (**a**) wild type and (**b**–**d**) the three Sin1 knockout clones. Due to the inverse contrast, silica has a light gray or white color, and pores through the silica and the background appear dark

gray. Green line = costa, orange line = cross-connection, red circle = areola pore, yellow or blue circle = fultoportula. Note that cross-connections are largely absent in the knockout mutants. SEM images extracted from the movies that were recorded during the displacement-controlled nanoindentation experiments of a single-cell wall from wild type and mutant knockout-1. (**e**–**g**) The wild-type images and (**h**–**j**) mutant knockout-1 compare the state of the cell walls from both specimens before, during, and after completion of the indentation experiment. The scale bars represent 1 μm [28].

Furthermore, Nemoto et al. [29] demonstrated that species-specific gene families play a crucial role in determining silica cell wall architecture. Through the comparative transcriptome analysis of *Nitzschia palea* and other diatom species, the research team identified a distinct gene family that responds directly to silica concentration in the environment. The transcriptome analysis revealed two key regulatory components: Sin1, the previously identified major protein involved in silica formation, and a novel SET domain protein methyltransferase family that shares homology with Sin1. Together, these genetic elements coordinate DB formation and ensure the structural stability of the cell wall. Significantly, the expression of these genes increased proportionally with environmental demands for silica accumulation, indicating an adaptive response mechanism. These findings reveal that diatoms possess sophisticated genetic networks that dynamically respond to environmental silica availability, suggesting that DB properties can be predictably modulated through environmental manipulation.

This environmental responsiveness, combined with the species-specific nature of these gene families, implies that different diatom species may serve as distinct biological platforms for producing DB with intended characteristics.

### *2.2. Ecological Functions of DB*

DB protects diatoms from mechanical shock or hydraulic pressure changes in the external environment and exhibit diverse morphological characteristics depending on the species [30,31]. In addition, the morphology of DB is considered an important classification key for traditional species classification, and their mechanical properties and hierarchical porous structure from the surface to the interior provide them with functionality, so that they can be applied in various industrial fields [32]. Their morphologies show diverse and elaborate geometric patterns, such as three-dimensional structures (e.g., cylinders, spheres, and lunates) with unique porous nanopatterned structures imprinted on their surfaces, planar structures (radial, navicular, elliptic-lanceolate, and stellate), and needle-like structures (Figure 2) [33].

The unique DB morphological features of all diatomic species are thought to be a means of adaptation to the environment [34]. Planktonic diatoms tend to have streamlined, elongated, or discoid morphologies that reduce their sinking velocities and maximize their exposure to sunlight for photosynthesis [35]. In contrast, sessile diatoms often have more robust and complex structures that enable them to withstand turbulent water and attach to substrates [36]. In habitats with high predation or turbulent water, certain diatoms develop thicker shell projections as a protective mechanism, and this strategy has been reported to reduce their vulnerability to physical damage [37]. These properties of DB morphology have provided valuable insights for biomimetic engineering applications. Musenich et al. [38] demonstrated a successful case of enhancing the performance of triboelectric nanogenerators by mimicking the morphological structure. DB functions as an electron acceptor, where its structural heterogeneity and high surface charge density maximize charge separation efficiency at the triboelectric interface, and it is successfully integrated into self-powered breath monitoring mask-type sensors. This morphological

mimicry extends beyond mere material substitution, presenting a concrete industrial biomimetic strategy where the structural design itself serves as the core mechanism for functional implementation.

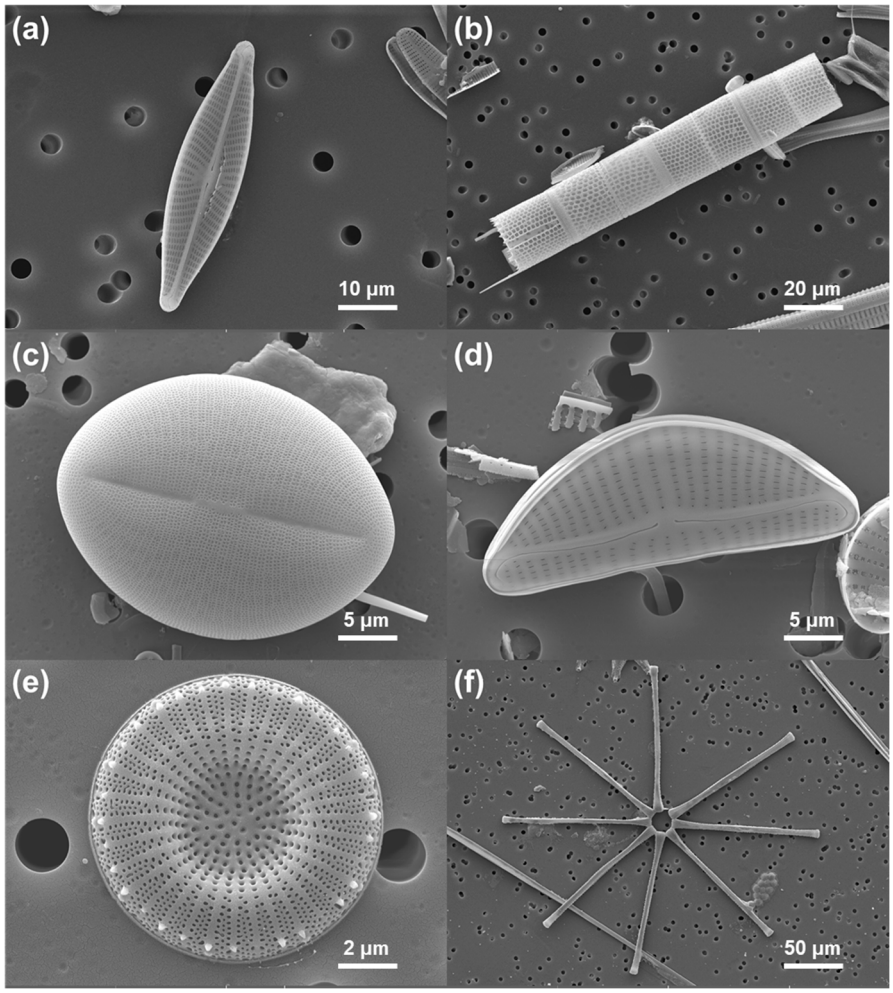



**Figure 2.** Field emission scanning electron microscope analysis results of DB show various morphological types: (**a**) navicular, (**b**) cylindrical, (**c**) elliptic-lanceolate, (**d**) lunate, (**e**) discoid, and (**f**) stellate morphologies.

Christian et al. [30] hypothesized that DB is an evolutionary product of the arms race and serves as an effective structural element for external mechanical protection owing to its mechanical strength. To verify this, we measured the force required to fracture single living cells of *Thalassiosira punctigera*, *Coscinodiscus granii*, and *Fragilariopsis kerguelensis*. Mechanical strength and cell size were found to be inversely proportional, with 730 μN, 260 μN, and 90 μN required to fracture *F. kerguelensis*, *T. punctigera*, and *C. granii* with respective sizes of 30, 50, and 130 μm. Simulation of the DB stress distribution for *F. kerguelensis* showed that the pressure distribution was biased toward the transversely arranged structures among the porous structures of the diatoms; when these structures were removed, the cells were fractured using only 60% of the measured force [30]. These results suggest that the outer cell wall of diatoms is not a simple biological barrier; instead, it acts as an excellent cell wall manifested by the microstructural evolution optimization [24]. In addition, the results show that the force required for crushing is different for each size, and that the specific structure of diatoms is a major supporting element for mechanical strength, providing a starting point for borrowing natural design principles in the development of biomimetic materials and microstructural designs.

The solid cell bodies of diatoms can also swim to adjust to light for photosynthesis and adapt to environmental changes. Karen et al. [39] reported that the raphe, a special slit in the DB, plays a key role in diatomic mobility (Figure 3a). Diatoms randomly select various movements (e.g., glide, reverse, pivot, and stop) (Figure 3b), and the diversity of these movement patterns implies adaptation to ecological niches and distinct mobility strategies in nature based on habitat and morphological diversity (Figure 3c). This suppresses competition with conspecifics while allowing diatoms to utilize important resources efficiently [39]. Thus, DB has a profound effect on the environmental adaptation of diatoms and helps diatoms play a stable role as major primary producers in terrestrial ecosystems.

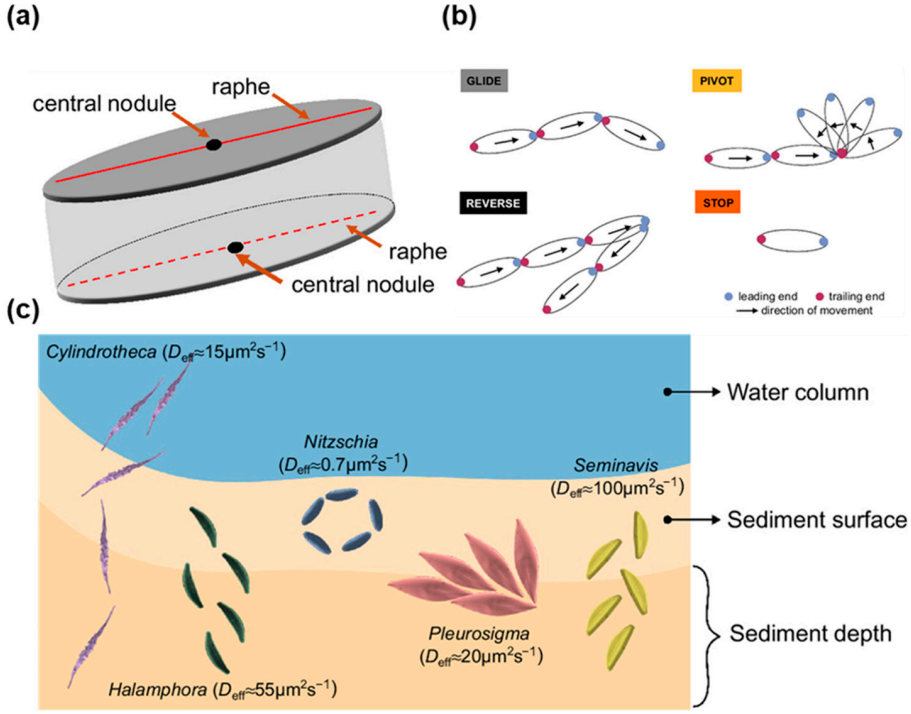



**Figure 3.** (**a**) Schematic image of a diatom. Red solid and dotted lines represent the raphe. The raphe is present on both the top and bottom valves of the cell. (**b**) Definition of the four possible states of diatom motility. (**c**) Schematic of diatoms' vertical migration highlighting the different ecological niches they inhabit [39].

### *2.3. Environmental Stimuli for DB*

Optimal growth conditions for diatoms are the most important factors for supplying DB, including external factors such as light, temperature, pH, salinity, and silicate concentration. Light intensity is a key factor that directly affects photosynthetic efficiency and DB production in diatoms [40,41]. Under optimal light intensity (typically 100–200 μmol $m^{-2}$ $s^{-1}$), the photosynthetic electron transport chain is optimized, maximizing ATP and NADPH production, which leads to increased carbon fixation rates and promotes DB accumulation [42]. However, when the photoinhibition threshold is exceeded, the D1 protein of photosystem II becomes damaged, causing a sharp decline in photosynthetic efficiency, and the cells consume energy for repair processes, thereby inhibiting DB accumulation [43]. In the study by Palanisamy et al. [44], the effect of blue light on the cell number of *T. pseudonana* was evaluated at 40 to 200 μE $m^{-2}$ $s^{-1}$, and the maximum cell number was shown to be twice that of 200 μE $m^{-2}$ $s^{-1}$ at 120 μE $m^{-2}$ $s^{-1}$. Despite the increased light intensity, the decreased cell growth rate was thought to be due to the increased cellular stress caused by the damage to the photosystem and the accumulation of reactive oxygen species (ROS) at light intensities above the saturation point [45]. Therefore, the characteristics of light, which vary considerably with water depth, may reflect the ecological conditions of diatoms,

which regulate photosynthetic reactions depending on the wavelength [46]; thus, they must be considered when designing a culture system. In addition, blue light induces stronger activation of photoprotective and photosystem II repair-related genes than that induced by green and red light [44].

Temperature affects the intracellular enzyme activity, photosynthetic rate, cell division cycle, and silicate uptake capacity of diatoms [21]. Most marine diatoms grow most actively at 20–24 °C; within this temperature range, photosynthetic enzymes such as rubisco and metabolic inducers such as adenosine triphosphatase and nicotinamide adenine dinucleotide phosphate synthase are actively expressed, which allows for efficient photosynthesis and biosynthesis [21]. In addition, cell cycle regulatory genes are actively expressed at optimal temperatures in each species, leading to regular cell division and DB formation [47]. According to actual experimental results, representative marine diatoms, such as *Phaeodactylum tricornutum* and *T. pseudonana*, exhibit maximum growth rates at 20–22 °C; during this time, the increase in cell density and the silicate consumption rate are maximized, showing enhanced DB accumulation at the optimal temperature [48]. The reaction rates of key enzymes involved in photosynthesis and metabolism decrease in low-temperature environments, whereas ROS are generated in diatoms under high-temperature conditions [49]. Therefore, temperature is a key factor that extends beyond the simple growth rate control factor and affects the amount and structural completeness of DB. In addition, pH and salinity are important environmental growth factors that vary among species and activate cellular metabolic activities within an appropriate range, affecting the diatomic growth rate, silica deposition, morphology, and size. pH directly affects DB production efficiency by determining the form and availability of inorganic carbon, thus directly influencing carbon fixation efficiency, while salinity affects DB production by determining the physiological state of cells through osmotic regulation and ionic balance [50–58]. This mechanism can be determined by complex environmental conditions such as light and temperature (Table 1).

**Table 1.** Effect of various culture conditions on diatoms.

| Condition | Species | Range | Effect | Reference |
|---|---|---|---|---|
| pH | *Fragilaria crotonensis* | 7.7 | Enhanced growth rate and silica accumulation. | [50] |
| pH | *Thalassiosira* sp., *Skeletonema* sp., *and Chaetoceros* sp. | 8.5 | Enhanced growth rate. | [51] |
| pH | *T. weissflogii* | 7.8 | Enhanced silicate accumulation. | [52] |
| pH | *Fragilariopsis cylindrus* | 8.1 | Enhanced growth rate | [53] |
| Salinity | *Cyclotella meneghiniana* | 18 PSU | Enhanced growth rate and silica accumulation | [54] |
| Salinity | *Skeletonema subsalsum* | 0–12 PSU | As salinity increases, the length of diatoms decreases, and their diameter and pore size increase. | [55] |
| Salinity | *T. pseudonana*, *Chaetoceros muelleri* | 36 PSU | Enhanced silicate accumulation | [56] |
| Temperature and salinity | *T. pseudonana* | 23 °C and Si limited<br>14–23 °C and Si replete | Enhanced silicate accumulation. | [57] |
| Light and salinity | *P. tricornutum* | 50:50 Red:Blue LED and 3.0 mM $Na_2SiO_3$ | Enhanced growth rate | [58] |

### *2.4. Purification*

Diatoms contain various organic substances, such as carbohydrates, proteins, lipids, and sterols, which are the center of metabolic activity; however, the removal of these internal organic substances is necessary for biomedical applications of DB [59]. Conventional methods for obtaining purified DB involve treatment with acids, hydrogen peroxide, or oxidizing agents, such as detergents (e.g., sodium dodecyl sulfate and ethylenediaminetetraacetic acid (EDTA)) [60]. Acids can easily remove the internal organic substances of DB, but can affect the dissolution rate of DB. In addition, it is difficult to remove the adsorbed inorganic cations; therefore, a post-treatment process is required to remove the inorganic cations that delay silica dissolution *via* EDTA and oxalic acid chelation [61]. In addition, traditional acid-based purification methods use high doses of strong acids or bases, which pose an environmental risk owing to their waste reagents.

The substances used for DB purification must be considered for their possible impact on the environment and human body, and substances that may have adverse effects must be minimized. In this context, eco-friendly purification approaches are gaining increasing attention as sustainable alternatives to conventional harsh chemical treatments. Peyman et al. [62] proposed the sono-Fenton (SF) process, which utilizes the synergistic effect of ultrasonication and an environmentally friendly Fenton reagent ($Fe^{2+}/H_2O_2$), leaving water and oxygen as the final products (Figure 4). This not only ensures effective purification but also minimizes toxic residues and environmental impact. The SF process promotes the generation of hydroxyl radicals through ultrasonic cavitation and increases the oxidative decomposition of organic matter attached to DB by inducing temporary high-temperature and high-pressure conditions achieved by the rapid vibration of microbubbles in the reaction medium. This process exhibits optimal efficiency at 45 °C, and is performed at a conventional temperature that is half of 90 °C. It was confirmed that the DB treated with the SF process had a more effective removal of impurities than the untreated DB (Figure 5a,b), and the weight percentage changes of C and Si shown in the energy-dispersive X-ray spectroscopy (EDX) spectrum and quantitative results emphasize the effective removal of organic substances from the purification process (Figure 5c,d) [62].

Ultrasonication can be applied as an effective strategy to enhance the purification ef-ficiency of DB. However, excessive treatment intensity or prolonged exposure may lead to the damage of DB itself [63]. Thus, optimization of sonication parameters, particularly intensity and duration are critical to balancing purification efficacy with structural preservation. Rossella et al. [64] demonstrated that under milder sonication conditions (Conditions A and B), most DB from *P. multistriata* remained intact. In contrast, more intense conditions (Conditions C–E) resulted in progressive structural degradation, with up to 70% of DB destroyed under Condition E (Table 2). Notably, this condition also allowed for the successful extraction of preserved nuclei, suggesting that controlled ultrasonication can serve not only as a purification tool but also as a targeted extraction method for intracellular biomolecules such as lipids, nuclei, and proteins. These findings underscore the importance of identifying a practical threshold balancing sufficient energy input to achieve purification or extraction goals while avoiding irreversible structural compromise.

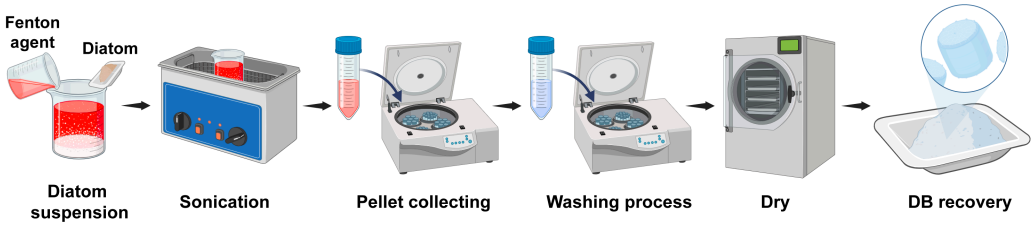



**Figure 4.** Schematic illustration of eco-friendly SF method for DB purification.

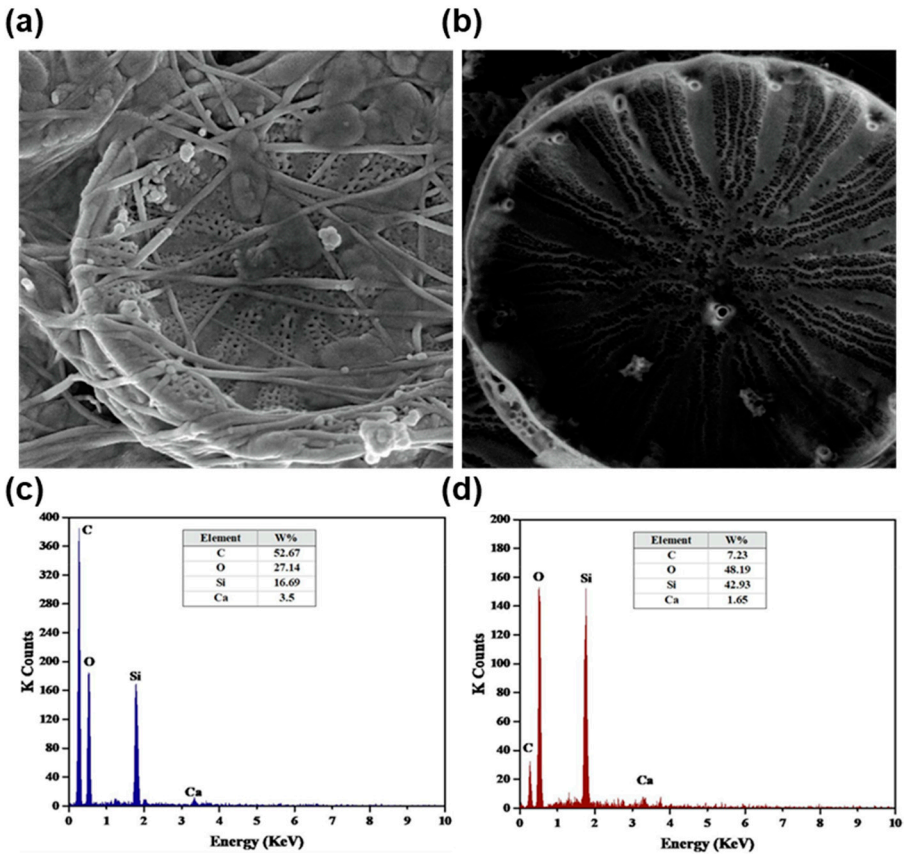



**Figure 5.** (**a**) SEM image of pure DB and (**b**) purified DB by SF process. The scale bar represents 2 µm. EDX spectrum analysis of (**c**) pure DB and (**d**) purified DB by SF process [62].

**Table 2.** Different combinations of sonication time for DB purification [64].

| Condition | $NH_4F$ Reaction Time | Sonication Power (W: Watt) | Pulse Condition |
|---|---|---|---|
| A | 3–5 min | 20 W | 1 pulse every 30 s for 3 min |
| B | 3–5 min | 40 W | 1 pulse every 30 s for 3 min |
| C | 10 min | 20 W | 1 pulse every 30 s for 3 min |
| D | 10 min | 40 W | 1 pulse every 30 s for 2 min |
| E | 10 min | 40 W | 1 pulse every 15 s for 3–11 pulse |

## 3. Application of DB in DDS

The hierarchical porous structure and surface functionalization characteristics of DB exhibit great advantages for application in DDS, which are suitable for high-drug loading efficiency and sustained-release formulations, as required by various newly developed poorly soluble drugs. Functionalization of DB through genetic modification and ligand attachment enables precise targeted delivery, demonstrating the potential of DDS as a new delivery platform. In this section, we discuss the functional characteristics of DDS, examine the possibility of *in vivo* degradability, and review the potential applications that can be used in the therapeutics field.

### *3.1. Sustained Drug Release*

The unpredictable drug burst release that occurs in the body can cause toxic effects, owing to the exposure of high drug concentrations to nontarget sites; thus, sustained release formulation studies have been conducted to address this issue [65,66]. Sustained and stable drug release kinetics are a key goal of DDS, as they reduce the side effects

caused by burst drug release and ensure consistent therapeutic levels [67,68]. DB has a shell composed of a silica-based mesoporous hierarchical structure [69]. Drugs are typically adsorbed onto the pores on the surface of DB and flow through the pores, binding to the internal microstructure [70]. This can be achieved through various mechanisms, including physical adsorption, electrostatic interactions, and covalent bonding [13,22]. Current strategies for drug-loading onto DB predominantly rely on passive diffusion and surface adsorption, which may limit both loading efficiency and the ability to modulate release kinetics. Therefore, the development of a drug-loading strategy that considers the physicochemical properties of therapeutic agents is essential. Covalent conjugation using silane coupling agents such as 3-aminopropyltriethoxysilane (APTES) can enhance the stability of drug immobilization [7]. In addition, non-covalent strategies, including electrostatic complexation *via* chitosan coating and hydrogen bonding interactions facilitated by polydopamine functionalization can be employed to strengthen drug–DB interactions while enabling controlled release [71,72]. The hierarchical structure of DB has been reported to complicate the diffusion path of the loaded drug, thereby improving its sustained release of the loaded drug [71]. The release mechanism of drugs loaded into DB is thought to be greatly affected by the diffusion of the drug and pore size [73]. To verify drug loading, Thi et al. [74] analyzed the structural characteristics of DB before and after doxorubicin incorporation using the Brunauer–Emmett–Teller (BET) analysis. The BET analysis results showed a marked reduction in surface area and pore size, indicating that doxorubicin was successfully adsorbed onto the DB surface and within its porous architecture (See Figure 6a,b for quantitative BET data).

Abhisheck et al. [70] loaded curcumin, a poorly soluble drug, into a DB obtained from *Thalassiosira weissflogii* and analyzed its release characteristics by natural diffusion along a concentration gradient. The drug exhibited a maximum loading efficiency of 79.05% in DB, and the release profiles of the loaded drug were characterized using the Higuchi and Korsmeyer–Peppas models. Both models were constructed under acidic (pH = 5.2) and physiological (pH = 7.4) conditions. In the Higuchi model, the regression coefficients of the drug release data observed under slightly acidic and physiological conditions were $R^2$ = 0.93 and $R^2$ = 0.96, respectively (Figure 6c). In the Korsmeyer–Peppas model, these coefficients were $R^2$ = 0.99 at pH = 7.4 and $R^2$ = 0.86 at pH = 5.2 (Figure 6d), confirming that controlled release occurred by diffusion-controlled release. However, in the free drug case, both models exhibited rapid drug release responses (Figure 6e,f). This provides indirect evidence that the surface of DB provides an excellent drug adsorption limit and improves encapsulation efficiency, and that van der Waals and electrostatic interactions between drug molecules, and the carrier matrix can improve sustained drug release [70]. Furthermore, the drug release profiles correlated with the pore size. According to Ormerod et al. [75], the release time as a function of pore size exhibited an exponential relationship, which was observed through the Robin boundary model targeting hydrophobic drugs. When the relative ratio of the drug (transferred from the inner parts of DB to the surface) was fixed at one, it was expressed as a function of x in the form of $1192e^{-0.6685x}$, where x represents the pore size. Accordingly, in the model, the time required for 90% of the hydrophobic drug to be released exhibited an exponential relationship with pore size, as a function of the release time and pore characteristics. These results emphasize that the hierarchical porous structure of DB is a potential biomaterial that can exhibit a gradual drug release effect by providing a large surface area suitable for drug loading and a structural environment in which the drug loaded inside is difficult to release.

However, current research on DB as a sustained release platform remains confined to the early developmental stages, with insufficient understanding of surface interaction mechanisms. In fact, the physicochemical properties of a porous structure and high specific

surface area alone cannot guarantee drug delivery efficacy, and there are limitations in accurately predicting the multifaceted interactions that occur in complex *in vivo* environments. Therefore, for the practical application of DB-based drug delivery systems, systematic studies must be conducted as prerequisites, including biodegradability assessment under various physiological conditions, *in vivo* stability validation, tracking studies, and stepwise clinical trial evaluations.

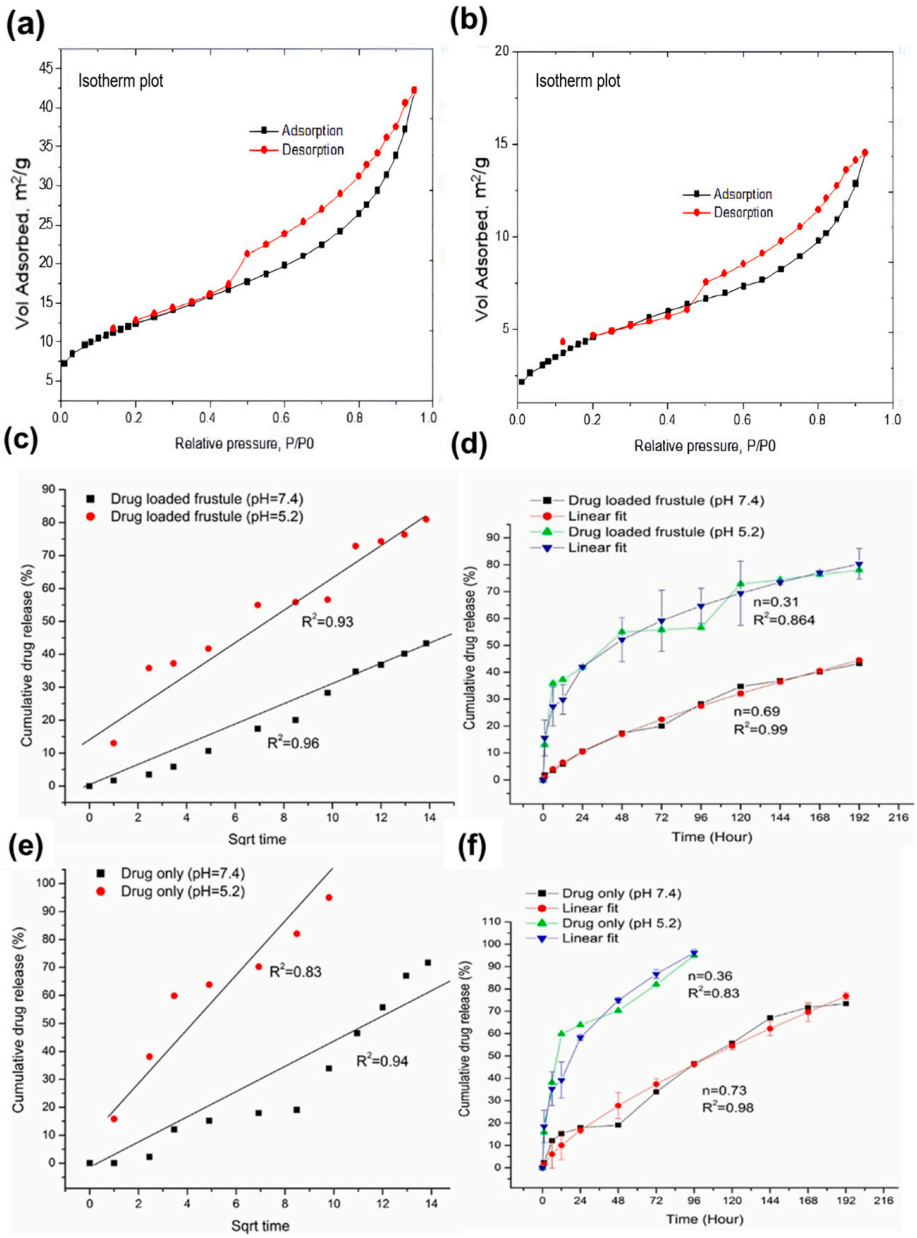



**Figure 6.** Nitrogen adsorption and desorption isotherms of (**a**) DB and (**b**) drug-loaded DB. The surface area of DB exhibited a decrease of 62.6% from 42.74 $m^2$ $g^{-1}$ (DB) to 15.96 $m^2$ $g^{-1}$ (after drug loading), suggesting that the drug was successfully loaded on the surface [74]. *In vitro* drug release profile of DB fitted to (**c**) the Higuchi model and (**d**) the Korsmeyer–Peppas model. Free drug *in vitro* release profile fitted to (**e**) the Higuchi model and (**f**) the Korsmeyer–Peppas model [70].

### *3.2. Targeted Delivery*

Targeted drug delivery is a core technology of DDS that aims to minimize side effects and improve treatment outcomes while delivering drugs directly to diseased tissues or cells [76]. DB is mainly formed by conjugating or coating targeting ligands, such as

antibodies and aptamers, on the outer parts of the carrier through chemical linkers or genetic modifications [77,78]. The abundant silanol groups and negative charge of DB facilitate their conjugation with various targeting ligands *via* chemical reactions [79]. Silica-based structures of DB can be modified through genetic engineering. Delalat et al. [13] synthesized an eco-friendly, targeted DDS for cancer cells by inducing the expression of an antibody-binding domain (GB1 of Protein G) on the surface of *T. pseudonana* DB. Using this binding domain, an antibody-conjugated genetically modified DB (GM-DB) was designed to selectively recognize and bind neuroblastoma SH-SY5Y and B-lymphoma cells. GM-DB delivered drug-loaded nanoparticles to cancer cells and exhibited selective anticancer effects; additionally, in the control group, normal fibroblast model BSR, cell viability was maintained above 90%, demonstrating high selectivity for cancer cells. Its performance was also evaluated in a neuroblastoma transplantation mouse model, in which a single intraperitoneal injection of the SN38 drug loaded onto biosilica (labeled with anti-p75NTR antibody) showed a 53% reduction in tumor size after 5 days. *In vivo* biodistribution studies showed that some degraded DB was observed in the liver and kidney sections, whereas no DB was found in the brain, heart, kidney, liver, lungs, or tail. Hepatic accumulation of DB is thought to result from the uptake of particles by macrophages in the reticuloendothelial system [13].

In addition to chemical-based targeting strategies, recent approaches have incorporated physical principles such as magnetism and environmental responsiveness to achieve spatially and temporally controlled drug release. Chao et al. [80] introduced DB microrobots modified on the surface of DB obtained from *Navicula* sp. using folic acid and amine groups to impart drug-release capability specific to neuroblastoma tumors. The DB microrobots were designed to have a pH-responsive targeted-release mechanism based on magnetism through $Fe_3O_4$ nanoparticles adsorbed on the surface and a weakly acidic environment formed in the cancer cell microenvironment. The dual drug loading strategy, integrating loaded cisplatin and paclitaxel, solved the multimodal treatment problem by synchronizing chemotherapy mechanisms. Notably, the dynamics of a magnetically loaded DB can be controlled by the three-dimensional magnetic field control system. The motion of the carrier can be regulated carefully according to different magnetic field conditions (Figure 7a–d), highlighting the potential advantage of controlling microrobots in various fluids *in vivo* based on the uniform distribution and release of drugs (Figure 7e) [80].

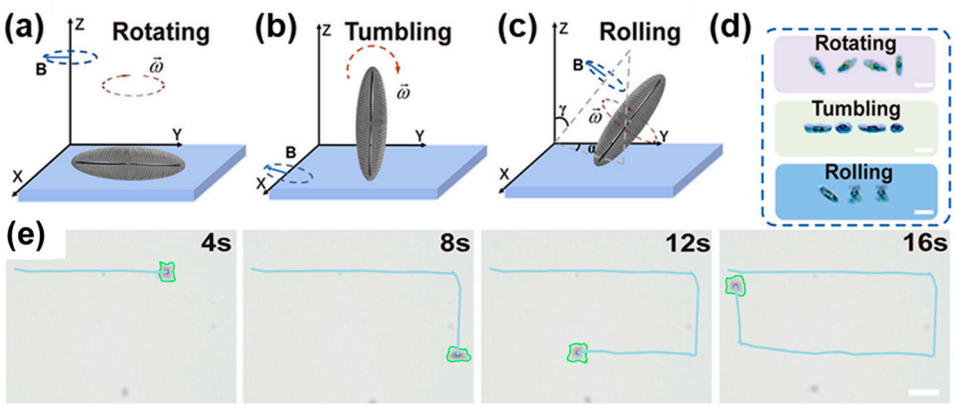



**Figure 7.** Motion modes and driving performance of the DB: (**a**) rotating mode, (**b**) tumbling mode, and (**c**) rolling mode. (**d**) Schematic images corresponding to the three modes; the scale bar represents 20 μm. (**e**) The DB is controlled to follow a rectangular trajectory in the rolling mode. The green box indicates the location of the DB. The scale bar represents 20 μm [80].

### *3.3. Biodegradability*

The toxicity of drug delivery vehicles administered *in vivo* needs to be evaluated over a long period, and verification of biodegradability is considered essential in the development of drug delivery formulation [81]. Verifying the biodegradability of DB is necessary to maximize the expected effects of its sustained release and targeting ability [9]. Despite the potential of DB as a sustained-release DDS platform, biodegradability studies on DB remain limited. To address this gap, future studies should involve *in vivo* experiments using animal models (e.g., mouse or rat) to track DB degradation kinetics in biological environments, as well as *in vitro* tests in simulated physiological fluids such as human plasma or lysosomal-mimicking buffers.

Therefore, in this study, we aimed to predict the biodegradability potential and efficiency of DB by evaluating the biodegradability of MSN, a silica-based DDS such as DB [82]. MSN, which has received Food and Drug Administration approval, has been evaluated as an appropriate material for application in the DDS field owing to its porous structure and various size distributions from nano- to microunits [83,84]. Kempen et al. [85] tested the biodegradability of MSN by dispersing 200 mL of synthesized 0.22 mg $mL^{-1}$ MSN in phosphate-buffered saline, followed by its concentration over time to perform transmission electron microscopy (TEM) imaging analysis [85]. MSN decomposition progressed over time after the measurement onset (Figure 8a–c), and an overall structural collapse occurred after 15 days (Figure 8d,e). In addition, most MSN dissolved after approximately 24 days (Figure 8f).

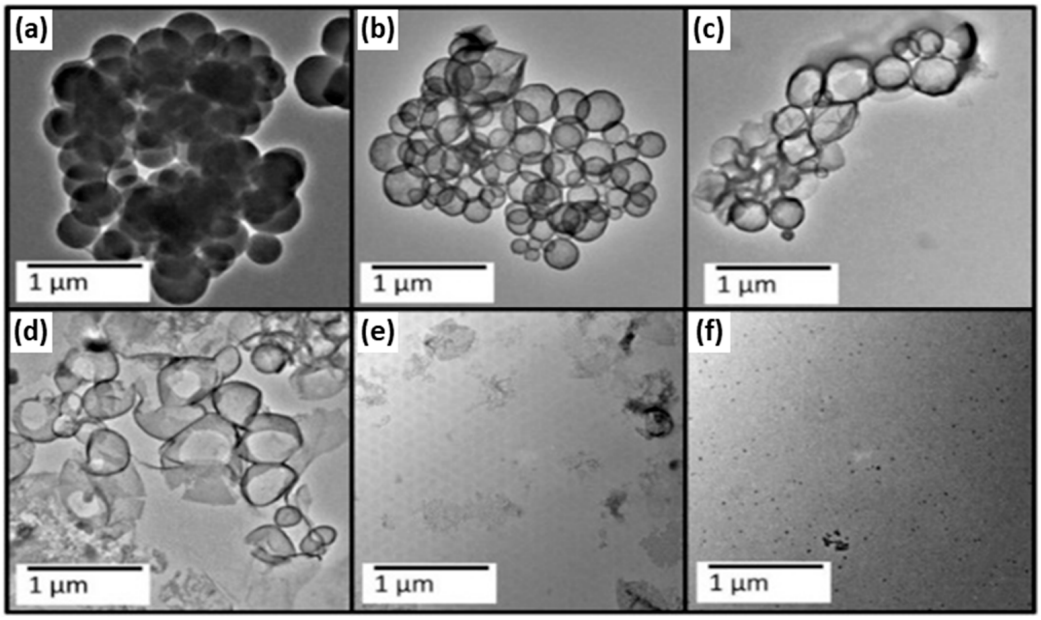



**Figure 8.** The retentate was collected and imaged with TEM at the following time points: 30 min (**a**), 7 days (**b**), 12 days (**c**), 15 days (**d**), 18 days (**e**), and 24 days (**f**). The MSN appears to be degrading from the inside out, with a hollow morphology appearing over time (**b**,**c**), finally collapsing upon itself (**d**,**e**) [85].

MSNs are generally considered crystalline materials, while DB is regarded as amorphous. A TEM-based fast Fourier transform (FFT) image analysis confirms that MSN possesses crystallinity, providing high durability and stability [86–88]. According to Spitzmüller et al. [89], this crystalline structure results in low biodegradability for silica particles. In contrast, FFT analysis reveals that DB exhibits an amorphous structure, which significantly enhances its biodegradability compared to crystalline MSN [90]. This amorphous nature makes DB sufficiently biodegradable within biological systems. Never-

theless, comprehensive experiments under various *in vivo* conditions are essential to fully validate biodegradability of DB, requiring in-depth exploration of degradation mechanisms rather than documenting degradation outcomes. DBs are a potential alternative that could exhibit similar efficacy to MSN (Table 3). Moreover, the development of scalable cultivation systems enables the continuous and environmentally sustainable recovery of DB, distinguishing it from synthetically derived MSN. In parallel, advances in pretreatment technologies may further enhance its biodegradability, thereby reinforcing its position as a superior candidate for biomedical applications [91].

**Table 3.** Comparison table of MSN and DB.

| Category | Material | Experimental Model | Property | Reference |
|---|---|---|---|---|
| Biocompatibility | MSN | *In vitro* | No significant apoptotic response in the splenic cell up to 100 μg/mL. | [92] |
| | DB | *In vitro* | No cytotoxicity in colon cells up to 100 μg/mL. | [93] |
| Sustained release | MSN | *In vitro* | After 12 h, approximately 40% of the drug was released. | [94] |
| | DB | *In vitro* | After 8 h, 68.5% of the drug was released from DB. | [95] |
| Biodegradability | MSN | *In vitro* | Degraded after 24 days in PBS. | [85] |
| | DB | *In vitro* | Degraded after 30 days in PBS. | [91] |
| Synthetic accessibility and cost | MSN | – | Surfactant-based and acid-base synthesis system offers a high-cost process. | [96] |
| | DB | – | Sustainable and eco-friendly biosynthesis-based culturing system offers a low-cost process. | [12] |

## 4. Use of DB in Biosensor

Biosensors combine bioreceptors and signal transduction systems to detect target substances and are extensively used in various fields, such as medicine, environment, food, and biosecurity [97]. The highly organized porous structure of DB enhances the sensitivity of the biosensor through its large specific surface area, which also provides favorable conditions for the adsorption and concentration of poorly soluble or hydrophobic molecules [98]. The excellent hygroscopicity of the DB plays an important role in allowing the bioreceptor to stably maintain its performance in a high-moisture environment, such as biological samples [99]. From the perspective of biosensors, these characteristics act as positive factors that selectively capture biomarkers in water and suppress nonspecific binding, thereby increasing the sensor [100]. DB-based platforms function as surface platforms or selective interactions, facilitating mediators that enable target molecules to interact effectively with bioreceptors.

The structural stability of DB improves its accessibility as a basic material for biosensor platforms, and stabilizes DB *in vivo*. Therefore, a DB-applied biosensor can secure high reproducibility and reliability even in biological sample environments (*in vitro*), such as plasma, body fluids, or cell culture media, which are mainly used in the diagnostic field [101]. Rapid and accurate signal detection is one of the most important factors in biosensor technology. To implement a precise sensing system, it is not sufficient to rely simply on specificity for target detection; detailed optimization of the chemical and physi-

cal properties of the sensor surface is required [102,103]. Accordingly, numerous research groups have been actively exploring the application of diverse scaffold materials to enhance and optimize sensor performance (Table 4). The compiled table presents a comparative analysis of various scaffold-based biosensors, evaluated against key performance parameters relevant to clinical and point-of-care diagnostics. These findings collectively underscore the potential of DB as a versatile and scalable scaffold material, positioning it as a promising alternative to synthetic nanomaterials in the development of next-generation biosensors. DB is highly compatible with various processes, such as the integration of functional molecules, surface modification, and chemical composition changes, enabling its expansion from a single target to a multitarget detection platform [104]. In this section, we organize various diagnostic strategies based on this DB-based biosensor platform using a measurement method and introduce its structural and functional applicability.

**Table 4.** Comparative characteristics of DB and conventional scaffold materials employed in biosensor platforms.

| Scaffold Material Properties | | | Biosensor Performances | | | Reference |
|---|---|---|---|---|---|---|
| **Material Type** | **Biocompatibility** | **Cost Efficiency** | **Detection Limit** | **Detection Range** | **Detection Method** | |
| DB | Biodegradable, low immunotoxicity; suitable for POC/*in vivo* use | Natural material-based, overwhelming cost efficiency | Under 0.1 ng/mL | Under 0.1 ng/mL | SERS | [105] |
| Graphene | High controllability in surface modification; applicable in neuro/cardiovascular biosensing | Cost effective | 1.15 ng/mL | 4–400 ng/mL | Differential pulse voltammetry (DPV) | [106] |
| Carbon nanotubes | Poor biocompatibility due to fibrous structure and ROS inducibility | High cost relative to performance | $8.15 \times 10^{-6}$ ng/mL | Under $8.15 \times 10^{-6}$ ng/mL | Field-effect transistor | [107] |
| AuNP | Low immunogenicity; biologically validated | Expensive; limited for large-scale use | 0.25 ng/mL | 1–500 ng/mL | LSPR | [108] |
| AgNP | Oxidative, cytotoxic; restricted in biomedical use | Inexpensive; requires oxidation stabilization | 0.57 ng/mL | 0.6–1 ng/mL | DPV | [109] |
| MXene | High-performing; long-term biocompatibility uncertain | Excellent requires optimization for cost-effectiveness | 0.29 µM | 0.5 µM–3 mM | Cyclic voltammetry (CV) | [110] |

### *4.1. Electrochemical Signal Detection*

Electrochemical biosensors detect target biomolecules based on electrical signal changes. Despite the relatively simple configuration of this sensing system, it is gaining attention owing to its high sensitivity and rapid analysis [111]. Cyclic voltammetry, electrochemical impedance spectroscopy (EIS), and potentiometric measurements are extensively used in various fields for diagnosis and monitoring [112]. The performance of electrochemical sensors is governed by the efficiency of mass transport and surface reactivity at the electrode-sensing interface, with the electrode material and structure of the surface being critical determinants [113]. DB has excellent porosity and a large specific surface area; therefore, when applied to an electrode, it effectively facilitates the adsorption

and diffusion of analytes [114]. These characteristics can be applied to increase the electron transfer efficiency and signal amplification strategy, thereby contributing to improved sensor performance. In particular, in a precision diagnosis environment where even a small number of target molecules must be effectively detected, this structural advantage is further highlighted because it exhibits a low-detection limit [115].

Silva et al. [116] analyzed the structural characteristics and electrochemical behaviors of DB-based composites to examine their potential as biosensors. The research team introduced various carbon sources (lignin, glucose, and activated carbon) to DB and combined them with magnetic nanoparticles to synthesize a new composite. The mixed and dried powders underwent a pyrolysis process using chemical vapor deposition, followed by mixing with alginate slurry and compression into a pellet form. The electrochemical properties of the manufactured composites were evaluated based on EIS and the I–V curve, and the tests were repeated to ensure the reliability and reproducibility of the sensor. As a result, the DB, activated carbon, and magnetic nanoparticles composite yielded the lowest resistance value of 0.09 Ω among the three carbon source combinations and exhibited the best electrical conductivity (Figure 9a,b). This was attributed to the transformation of activated carbon into a graphite-like structure during pyrolysis. In addition, the crystallinity and degree of graphitization of the carbon structures within the composites were evaluated based on the intensity ratio of the D band to the G band (ID/IG ratio) observed in Raman spectroscopy (Figure 9c). A lower ID/IG ratio indicates a lower density of structural defects and a higher degree of ordering in the $sp^2$-hybridized carbon network. Lignin and glucose, serving as a polymeric biomass precursor and a monosaccharide-derived carbon source, respectively, contributed to the formation of distinct carbon morphologies when incorporated with DB. Lignin, due to its aromatic and cross-linked macromolecular structure, yielded a more amorphous and disordered carbon framework upon pyrolysis. In contrast, glucose exhibited relatively homogeneous thermal decomposition behavior, promoting the formation of a more uniform and conductive carbon matrix. However, composites incorporating these two carbon sources demonstrated inferior performance in terms of electrical conductivity and structural integrity when compared to the activated carbon-based composite. This observation suggests that activated carbon underwent a more effective graphitization process during pyrolysis, resulting in the formation of a highly crystalline graphite-like structure, which facilitated more efficient electron transport within the composite. DB-based composite materials demonstrated consistent structural stability and uniform dispersion characteristics even when various carbon sources were introduced, indicating that the inherent porosity and surface properties of DB contributed to enhanced electrochemical performance [116]. These findings suggest that DB represents a functional platform with potential for application as a high-sensitivity biosensor material.

The structural uniqueness and multifunctionality of DB demonstrate their potential for high-performance biosensor applications [105]. When integrated with electrochemical devices, the enhanced sensitivity and selectivity offer broad practical applicability across diverse analytical scenarios [105]. Although research on DB-based electrochemical biosensors remains limited, their exceptional electrochemical behavior presents numerous opportunities for precise control mechanisms, integration with nanomaterials, and compatibility with microrobotic technologies [117]. Furthermore, because of their superior stability and functional adaptability, DB-based systems are expected to expand sensor applications in complex biological environments, enabling real-time monitoring and detection under challenging physiological conditions [101].

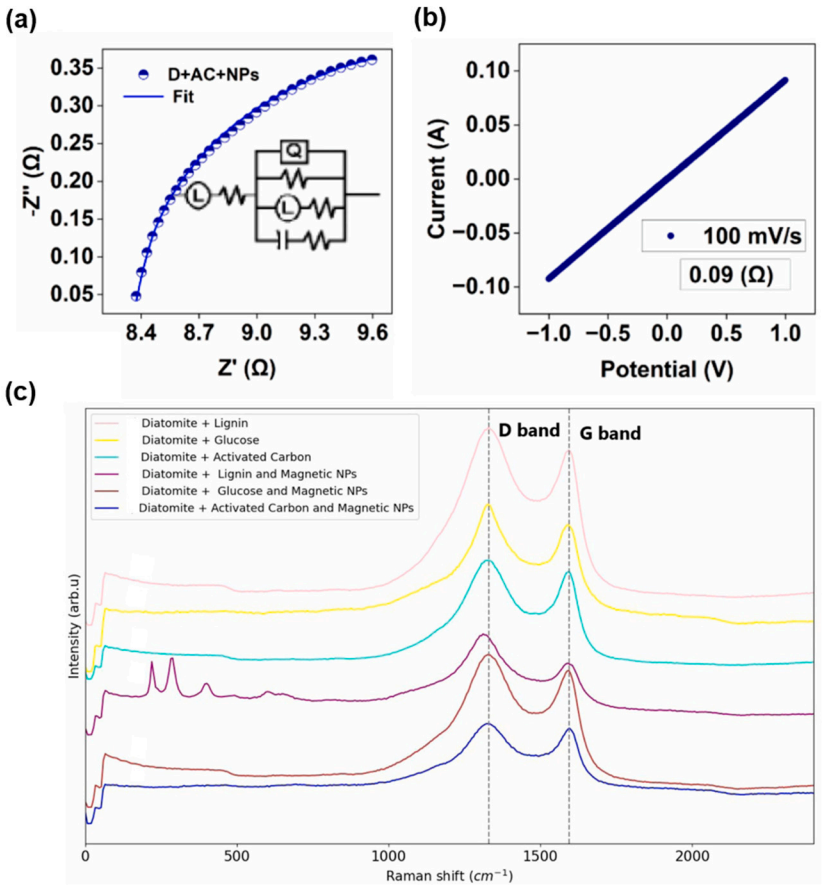



**Figure 9.** (**a**) Nyquist plot of DB, activated carbon, and magnetic nanoparticles (D + AC + NPs). (**b**) I–V curve of DB, activated carbon, and magnetic nanoparticles. (**c**) Raman spectra of composite materials after pyrolysis [116].

### *4.2. Optical Signal Detection*

Highly sensitive, real-time, and noninvasive analytical capabilities have established biosensor technologies as essential tools for biomedical diagnostics and monitoring. Among these technologies, optical biosensors have gained considerable attention because of their ability to detect biomolecular interactions directly using label-free methodologies [118]. DB possesses naturally formed, intricate silica-based nanostructures that provide a robust physical foundation for amplifying various optical phenomena, including light scattering, refractive index modulation, and surface plasmon resonance enhancement [119]. Based on these unique optical properties of DB, this section examines signal amplification mechanisms that can enhance the sensitivity and selectivity of biosensors, while presenting recent research trends and application cases that demonstrate the potential of DB-integrated optical biosensing platforms [120].

Saridag et al. [116] developed a DB-based, flexible sensing platform capable of the rapid and sensitive detection of cancer-specific protein biomarkers in serum using surface-enhanced Raman scattering (SERS). To facilitate electrostatic interactions with silver nanoparticles (AgNP), the DB surface was functionalized using silanization with APTES, introducing amine groups (-$NH_2$). The resulting AgNP@DB complex served as a structural foundation for SERS signal amplification, which was further enhanced by conjugating reporter molecules, such as Raman probes and specific antibodies for target protein recognition, thereby achieving immunoassay-based selectivity (Figure 10). The developed sensor demonstrated the accurate discrimination of major cancer proteins, including HER2, CA15-3, MUC4, and PSA (Figure 11a–d), with the SERS signal intensity exhibiting a distinct linear correlation with the protein concentration. The platform achieved detection limits

as low as 0.1 ng $mL^{-1}$, with clear signal differentiation, demonstrating exceptional sensitivity (Table 5). In addition, the minimal signal variation across repeated measurements confirmed excellent reproducibility. These performance characteristics are attributed to the synergistic effects of efficient surface adsorption facilitated by the high surface area of the DB and the strong electromagnetic field enhancement induced by AgNP [116]. These findings demonstrate that DB-based platforms effectively address the sensitivity and selectivity limitations commonly encountered in conventional inorganic material-based sensors, establishing DB as a promising substrate for advanced biosensing applications.

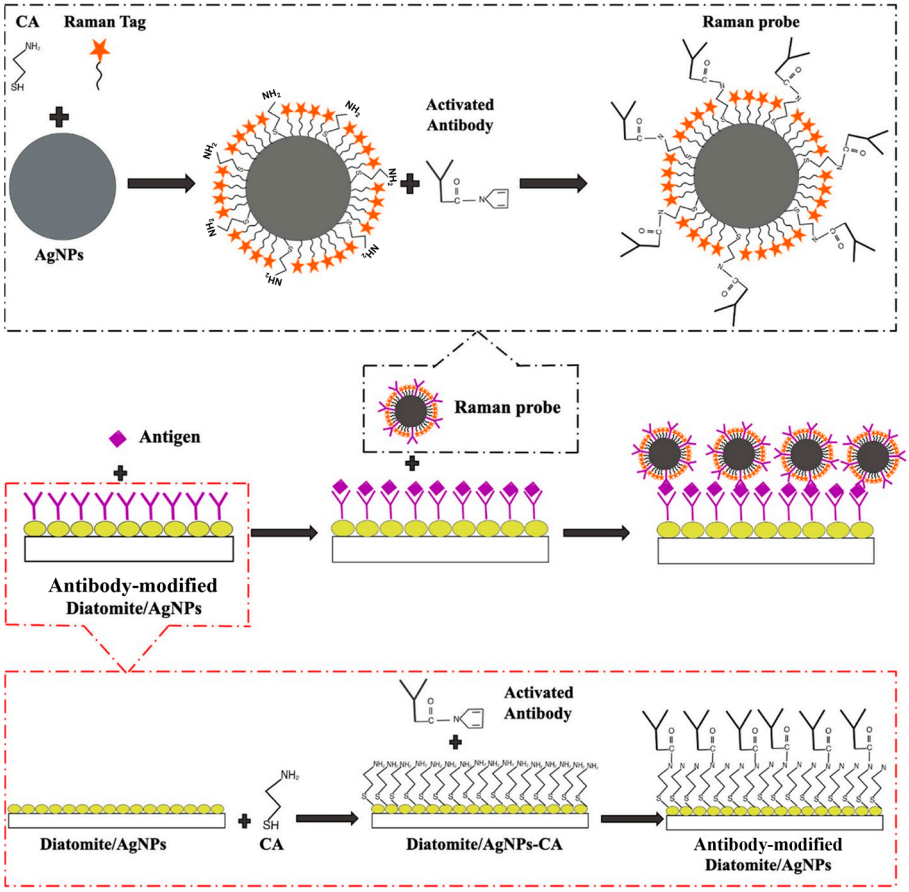



**Figure 10.** Schematic illustration of the sandwich immunoassay protocol for the detection of target antigens. The red-lined region represents a schematic representation of the modified DB/AgNP surface with the antibody. The black-lined region represents a schematic representation of the modified AgNP with cysteamine, a Raman tag, and an antibody [105].

**Table 5.** Summary of signal amplification and detection limits for SERS-based sandwich immunoassay [105].

| Target Antigen | Raman Marker Peak ($cm^{-1}$) | Calibration Curve Equation (y = ax + b) | Slope (Signal Amplification) | $R^2$ (Linearity) | LOD (ng/mL) |
|---|---|---|---|---|---|
| HER2 | 1579 | y = 18.346x + 602.7 | 18.35 | 0.948 | Under 0.1 |
| CA15-3 | 1333 | y = 82.76x + 1754.1 | 82.76 | 0.9703 | Under 0.1 |
| MUC4 | 1066 | y = 72.625x + 4578.6 | 72.63 | 0.9913 | Under 0.1 |
| PSA | 1333 | y = 175.96x + 3066.8 | 175.96 | 0.9995 | Under 0.1 |

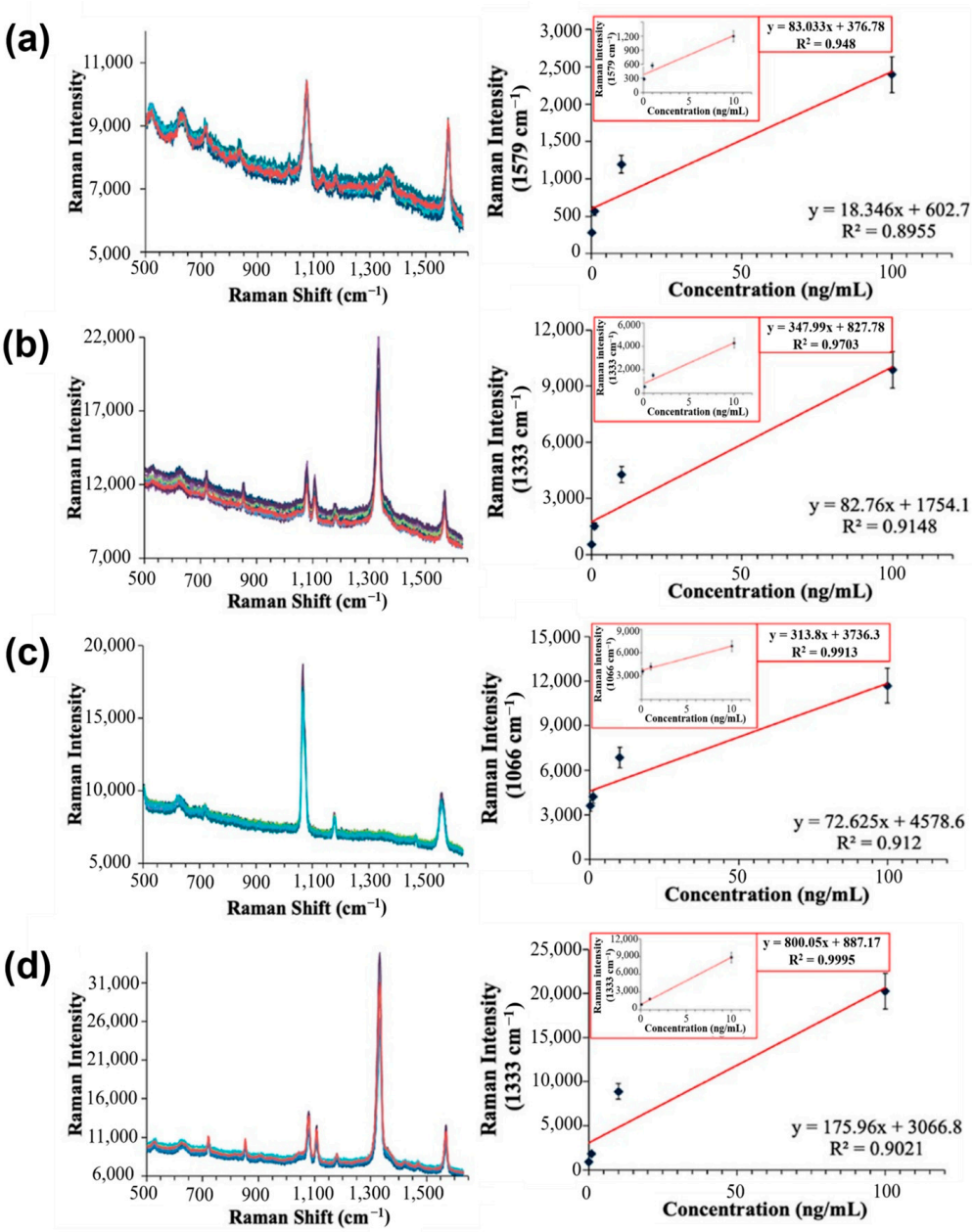



**Figure 11.** (**a**) Reproducibility of the spectra and calibration curves of the sandwich assay belonging to the HER2 antigen; (**b**) reproducibility of the spectra and calibration curves of sandwich assay belonging to the CA15-3 antigen; (**c**) reproducibility spectra and calibration curves of the sandwich assay belonging to the MUC4 antigen; and (**d**) reproducibility spectra and calibration curves of the sandwich assay belonging to the PSA antigen. Spectral graphs visually distinguish between experiments measured repeatedly under identical conditions. Higher spectral consistency indicates better reproducibility [105].

León-Valencia et al. [121] developed a DNA fluorescence biosensor by depositing AgNP on DB surfaces *via* photochemical reduction. Fourier transform infrared spectroscopy (FT-IR) analysis revealed the characteristic DB peak at 1003 $cm^{-1}$ in the synthetic complex, confirming that the DB structural integrity was preserved following nanoparticle deposition (Figure 12a). Upon DNA incorporation, additional peaks corresponding to N-H and C-N bonds were observed at 2974 $cm^{-1}$ and 1044 $cm^{-1}$, respectively, providing evidence for interactions of the nanoparticle and DNA. The unique architecture of DB facilitates the formation of plasmonic hotspots through localized electromagnetic field enhancement, which is a critical factor for sensitivity improvement. Raman spectroscopic

analysis demonstrated that DNA addition to AgNP-functionalized DB resulted in an approximately 5.5-fold signal enhancement at 440 nm, with the observed peaks consistent with the FT-IR findings (Figure 12b). These results indicate that the porous structure of DB effectively amplifies the plasmonic resonance, leading to a major enhancement in both the fluorescence and SERS signals. The synergistic combination of the hierarchical porous architecture of DB and AgNP-induced plasmonic effects established a robust platform for sensitive nucleic acid detection, demonstrating the potential of DB-based hybrid systems in molecular biosensing applications [121].

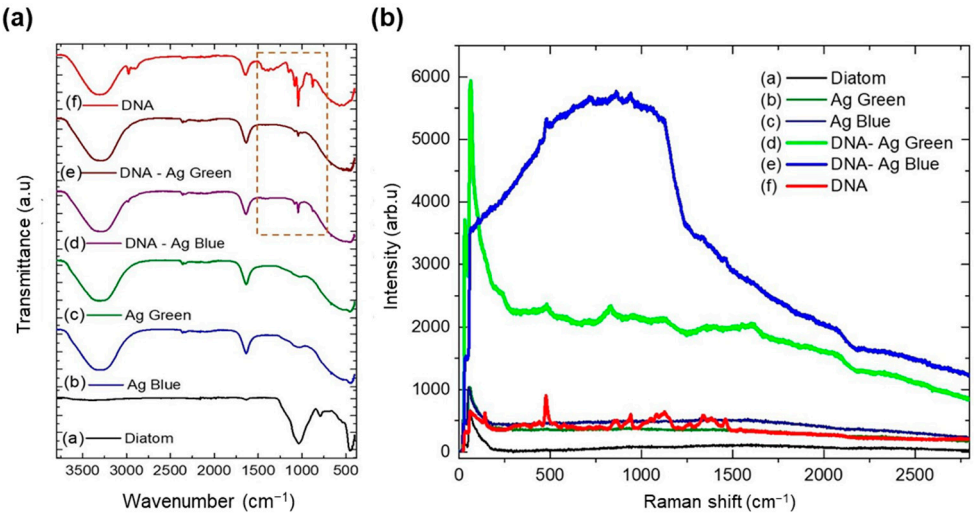



**Figure 12.** (**a**) FT-IR and (**b**) Raman spectra of DB, DB irradiated at 440 nm (Ag blue) and 540 nm (Ag Green), DB irradiated with DNA at 440 nm and 540 nm, and DNA pristine. The dotted brown boxes highlight C-O and C-N bindings [121].

Ide et al. [122] fabricated a buoyant photoreactive composite for water-floating applications by adsorbing single-walled carbon nanotubes (SWNTs) onto DB surfaces. The researchers stabilized the SWNTs with single-stranded DNA and subsequently immobilized them onto APTES-functionalized DB surfaces to form a composite structure. The optical performance was characterized, with a particular emphasis on the near-infrared luminescence properties (Figure 13a–d). The composite exhibited strong luminescence characteristics, with an absorption wavelength of 650 nm and an emission wavelength of 1100 nm. Notably, the luminescence intensity of the DB pretreated with Pipe Unish cleaner reached a maximum of 0.551, representing an approximately 55-fold enhancement compared to the untreated DB, which showed an intensity of only 0.01. This significant increase is attributed to the synergistic effects of enhanced SWNT adsorption efficiency and localized surface plasmon resonance (LSPR), both facilitated by surfactant-mediated surface modification. Furthermore, the resonant properties of the structured DB are thought to amplify the local electromagnetic field, thereby maximizing the sensitivity of the optical signal. Raman spectroscopy analysis revealed a graphitic-to-disorder band intensity (G/D) ratio of 6.67, which confirms the successful immobilization of SWNT, with preserved structural integrity (Figure 13e). A high G/D ratio indicates minimal disorder, demonstrating the effectiveness of the DNA-mediated stabilization approach. This composite, capable of floating on water surfaces while maintaining a strong optical signal output, demonstrates tremendous potential for diverse sensing applications, including water-quality monitoring and biosensing platforms. The combination of the natural buoyancy of DB with its exceptional optical properties establishes a unique sensing modality for aquatic environmental monitoring and waterborne target detection [122].

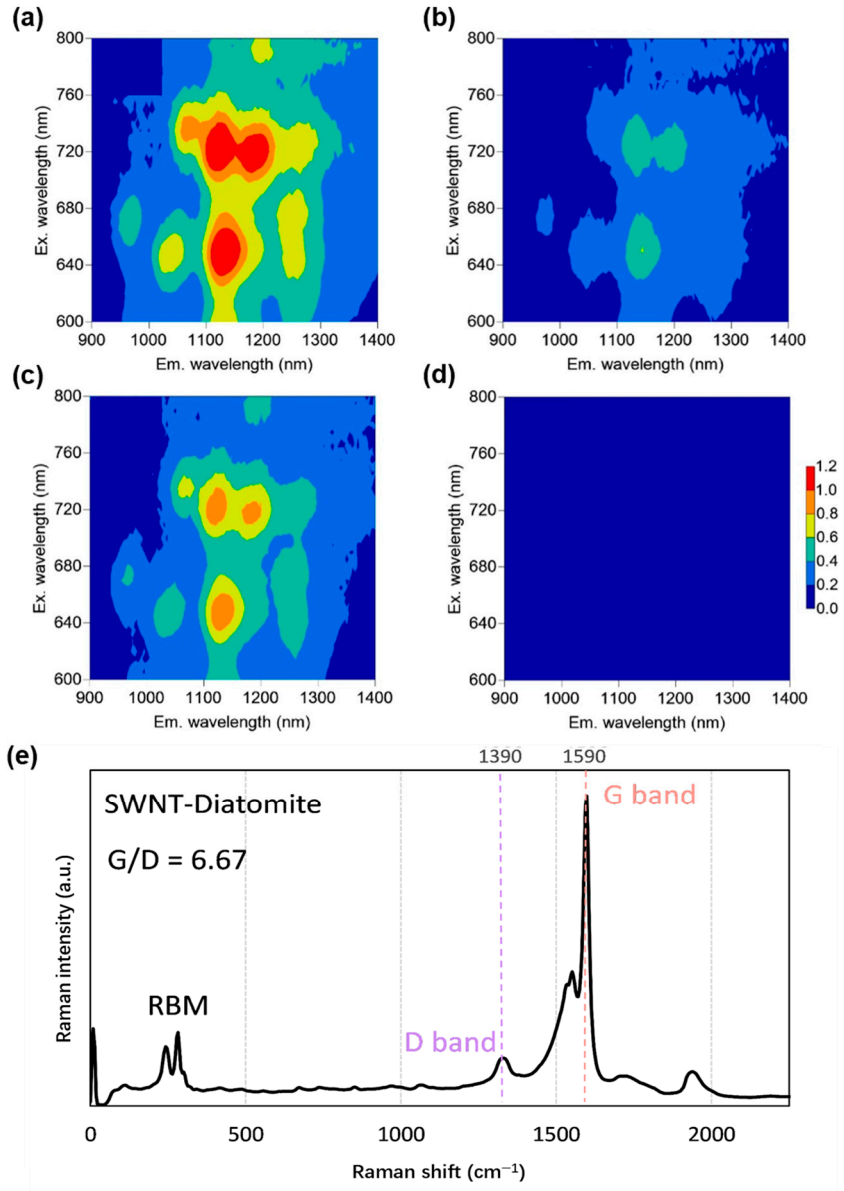



**Figure 13.** PL maps of single-stranded-DNA-SWNT hybrids and those attached to aminated DB surfaces. PL map of the DB surface treated with (**a**) Pipe Unish cleaner and APTES, (**b**) NaOH and APTES, (**c**) APTES, and (**d**) no surface treatment; (**e**) Raman spectra of single-stranded-DNA-SWNT hybrids [122].

The optical performance of DB-based platforms highlights their potential not only for clinical translation but also as scalable technologies for future commercialization. Notably, a DB-based photoluminescence (PL) immunosensor functionalized with gold nanoparticles (AuNPs) demonstrated a low limit of detection (LOD) of $8 \times 10^{-9}$ mg/mL and a broad dynamic range from $10^{-9}$ to $10^{-2}$ mg/mL, thereby achieving both high sensitivity and optical signal stability in a label-free manner [123]. Furthermore, a DB-enabled SERS immunoassay was capable of quantitatively detecting the inflammatory cytokine interleukin-8 (IL-8) in human plasma at concentrations as low as 6.2 pg/mL, representing a performance enhancement of several hundred-fold compared to the nanogram-per-milliliter sensitivity of conventional planar glass-based sensors [124]. These findings underscore the viability of photochemical signal amplification strategies as foundational technologies for the development and clinical deployment of point-of-care (POC) biosensing devices, supporting their future translation through clinical validation and regulatory approval.

The intricate and naturally formed silica structures of DB exhibit unique optical properties that are difficult to implement using existing artificial materials [125]. These distinctive characteristics effectively enhance the sensitivity and selectivity of the sensor by amplifying optical signals based on mechanisms such as light scattering enhancement, refractive index modulation, and plasmonic field concentration [126]. Despite the demonstrated potential of DB-based optical biosensors in recent studies, significant technical hurdles continue to impede their widespread implementation. Key challenges include maintaining structural homogeneity among different diatom species, developing robust surface functionalization methodologies, and ensuring compatibility with established analytical platforms [127]. Future developments should focus on overcoming these limitations through interdisciplinary approaches that combine advanced material engineering, precision microfabrication techniques, and artificial-intelligence-driven analytical platforms [120]. The integration of machine-learning algorithms for signal processing and pattern recognition, coupled with standardized DB preparation and functionalization protocols, is crucial for translating laboratory demonstrations into robust clinical diagnostic tools. Although DB-based optical biosensors are currently in the nascent stage, the convergence of their unique structural properties with emerging technologies makes them promising candidates for next-generation POC diagnostic platforms, particularly for applications requiring high sensitivity, rapid response, and cost-effective implementation.

### *4.3. Fluorescent Signal Detection*

Fluorescence-based detection has been extensively implemented in biosensing systems owing to its superior sensitivity and selectivity [128], and diverse technological strategies are being pursued to enhance signal intensities and stability. DB exhibits intricate hierarchically organized nanoporous architectures that provide optimal platforms for efficient fluorophore immobilization and uniform distribution [129]. Sophisticated DB structures that function beyond conventional physical scaffolds offer advantageous microenvironments for advanced applications, including intracellular fluorescence monitoring and functionalized interface-mediated target recognition [130]. When integrated with fluorescent probes or quantum dots (QDs), DB-based platforms enable localized signal amplification, considerably enhancing sensor performance metrics and demonstrating substantial potential for expanding the operational scope of current sensing technologies [131].

Mu et al. [132] investigated a simple biosensor fabrication strategy to construct a composite fluorescent sensor by conjugating CdSe/ZnS QD to DB surfaces. Notably, this conjugation was achieved *via* simple physical adsorption rather than conventional covalent bonding, thereby eliminating the need for complex surface functionalization or linker chemistry. This significantly streamlines the sensor fabrication process and offers a cost-effective approach for the large-scale production of fluorescent biosensors. Importantly, this approach not only preserved the intrinsic fluorescence of the CdSe/ZnS QD but also enhanced optical output by 1.26-fold, attributed to the high surface area and porous nanostructure of DB, which facilitated uniform CdSe/ZnS QD dispersion and improved light scattering. This indicates an improved LOD of the fluorescent probe. CdSe/ZnS QD were employed at a concentration of $7.5 \times 10^{-3}$ nmol $mL^{-1}$, a level shown not to interfere with diatom growth, and a positive correlation between QD binding and fluorescence intensity was observed. The CdSe/ZnS QD–DB composite exhibited emission peaks at 450, 560, and 680 nm, with confirmed spectral broadening and red-shift characteristics (Figure 14a,b). These spectral changes were attributed to the aggregation or size variations of the CdSe/ZnS QD upon binding to the DB surfaces. Collectively, this study highlights the potential for scalable, low-complexity fabrication of fluorescent biosensors under minimal synthetic constraints.

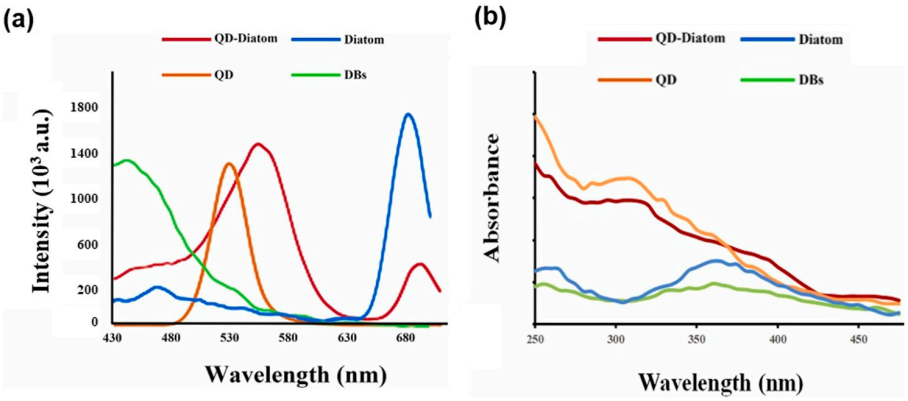



**Figure 14.** (**a**) A 380 nm emission spectrum and (**b**) optical absorption spectrum of diatom, DB, QD, and QD-diatom [132].

Wang et al. [133] developed an innovative microfluidic platform by integrating the nanoporous structures of DB within microfluidic chips and implementing a flow-through configuration in which analytes directly traverse the nanopores, resulting in effective fluorescence signal amplification. This approach enabled the development of a simple yet reliable POC testing device with potential extensions to smartphone-based sensing systems. The flow-through methodology demonstrated substantial performance improvements compared with conventional flow-over approaches (Figure 15a–d). Reaction times were reduced by up to 16-fold, even at low concentrations of 10.0 μg/mL, while computational simulations indicated approximately 29-fold enhancement in adsorption kinetics. The particle-tracing module of COMSOL Multiphysics simulations revealed that nanopores within the DB structures generate microflow perturbations that increase the particle–surface contact frequency, considerably improving the adsorption efficiency. Experimental validation confirmed the linear enhancement of the fluorescence signals at increasing flow rates, supporting the critical role of these structural characteristics in signal amplification. Concave DB geometries exhibited superior adsorption rates and sensitivity compared to convex configurations (Figure 15e–h), demonstrating the influence of structural morphology on performance metrics [133]. Furthermore, the etching process for achieving a regular array and customized geometric control was implemented based on established micro-electro-mechanical systems (MEMS) technology. Micro step-through holes with diameters of 115 μm and 75 μm, center-to-center spacing of 138 μm, and a depth of approximately 13 μm were precisely fabricated on a silicon substrate. This enabled the construction of a robust scaffold capable of spatially organizing DB into a highly ordered array. Such a structural configuration facilitates the uniform distribution of optical signal enhancement, minimizing localized bias and thereby maximizing resonance and scattering effects with high reproducibility and consistency. Consequently, this platform offers an optimized analytical environment for high sensitivity biosensing applications within microfluidic systems. These findings demonstrated that DB-based nanostructures function effectively as molecular concentrators and fluorescence amplifiers, and the flow-through approach provides a robust technological foundation for diverse fluorescence biosensor platforms, including immunodiagnostics and enzyme-linked immunosorbent assay-based analytical systems. DB-based fluorescent biosensors exhibit substantial potential for signal amplification and stability enhancement, making them promising platforms for analytical applications that demand high sensitivity and selectivity [129].

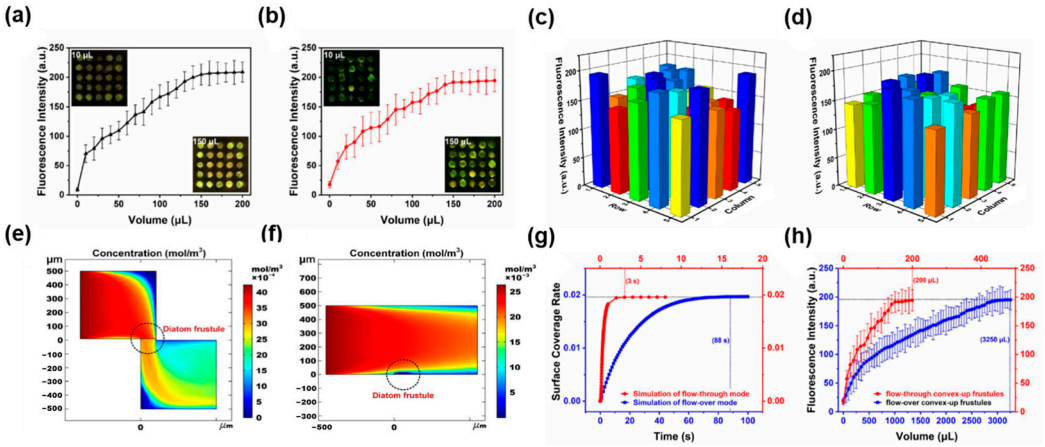



**Figure 15.** The average fluorescent intensity of (**a**) concave-up DB and (**b**) convex-up DB. The fluorescence intensity distribution of 25 DB of (**c**) concave-up orientation and (**d**) convex-up orientation.; Simulation results of concentration distribution of (**e**) flow-through, (**f**) flow-over detection, and (**g**) surface coverage rate of fluorescence molecules over time. (**h**) Smartphone analysis results of fluorescence intensity of flow-through and flow-over for convex-up DB [133].

DB has garnered considerable attention as a next-generation biosensing platform due to its intrinsic nanoporous architecture and biological origin. However, several limitations still hinder its practical application. One primary challenge is the difficulty in precisely controlling the functionalization and surface modification of the intricate nanoporous surface of DB, which can significantly compromise the sensitivity and specificity of selective biomolecular recognition [123]. Chen et al. [123] highlighted that the inherent chemical inertness of the DB surface restricts its utility in immunoassays. To address this limitation, -$NH_2$ were introduced onto the DB surface *via* surface treatment with 3-aminopropyltrimethoxysilane (APS), followed by covalent conjugation with rabbit immunoglobulin G (IgG). Furthermore, the biosensing performance in label-free detection was enhanced through conjugation with AuNPs, demonstrating improved analyte recognition capabilities. Another structural limitation of DB lies in its morphological heterogeneity, which arises from species-specific diversity related to the diverse biological functions of diatoms [134]. This heterogeneity results in inefficiencies, as it necessitates extensive screening and selection to identify DB structures suitable for specific biosensing applications. In response, Sun et al. [134] proposed a biofabrication strategy that incorporates both biological manufacturing processes and regulatory control mechanisms. By manipulating environmental and genetic factors, they established a scalable method for producing DB with standardized architectures. This strategy is expected to play a pivotal role in enabling large-scale production and facilitating the commercialization of DB-based biosensors.

The distinctive hierarchical porous silica architecture of DB provides effective scaffolding for fluorophore immobilization and uniform distribution, thereby contributing to enhanced signal intensity and optical performance [135]. However, successful commercialization requires addressing several technical challenges, including structural consistency across different diatom species, precise control over surface functionalization protocols, and scalable manufacturing processes [136]. Future research endeavors will be instrumental in overcoming these limitations and expanding the application scope of DB-based fluorescence sensing technologies to diverse domains, including the life sciences, environmental monitoring, and clinical diagnostics [131].

## 5. Theragnosis

The development of biomaterials is expanding beyond simple diagnostic or therapeutic functions to multifunctional platforms that can perform both functions simultaneously [137–139]. Theragnosis is a convergence concept that involves the diagnosis and therapy of diseases and is receiving attention as a precision medicine approach that can maximize treatment efficiency and minimize side effects [140,141]. Recently, extensive research has been conducted on theragnostic systems based on various biomaterials, including nucleic acids, lipids, proteins, and polypeptides, which are utilized as useful carriers and diagnostic probes in these systems because of their high biocompatibility and biodegradability [142–145].

For example, aptamer-conjugated liposomes and enzyme-responsive protein cages enhance target specificity and enable precise treatment that responds to the microenvironment of specific diseases, such as cancer [146,147]. However, single biomaterial-based systems have limitations in terms of durability, controllability, and production process, and fusion with various inorganic nanomaterials is being attempted to overcome these limitations [148,149]. MSN is used in theragnosis research owing to its large surface area, high porosity, ease of surface modification, easy loading, and controllable drug release [150,151]. MSN can simultaneously load fluorescent probes, magnetic resonance imaging contrast agents, photosensitizers, and anticancer drugs with high-loading efficiency, allowing for the integration of diagnostic and therapeutic functions [152,153]; they are also suitable for implementing smart release systems that respond to various biological environmental stimuli, such as pH, enzymes, and temperature [154]. Despite these advantages, MSN is associated with a complex synthesis process and environmentally hazardous because of the toxic reagents used; however, there are still limitations in securing biocompatibility and biodegradability for clinical applications [155].

Therefore, the possibility of developing a theragnostic platform using silica materials that are more eco-friendly and biocompatible than MSN has been suggested. DB has attracted considerable attention as a representative alternative [67,156]. DB can secure various types of sophisticated porous silica structures through species selection according to the desired purpose [157,158]. In addition, while sharing many of the aforementioned advantages of MSN, DB is differentiated by its bio-based production method, environmental friendliness, and potential for mass production [22,130]. The unique properties of DB secure various functionalities through genetic modification, including targeting ability, suggesting that they can be applied to anticancer, anti-inflammation, and various pathogenic molecular diagnostics [13,105,124]. These functionalities include multiple roles essential for theragnosis, such as diagnosis, drug binding, and the configuration of stimulus-responsive release systems [159,160]. These advantages provide grounds for DB to be considered a natural biomaterial for the development of next-generation theragnosis platforms that can overcome the limitations of existing synthetic materials. In summary, DB is expected to develop into a material that will lead to the development of precision diagnosis and treatment technologies as a hybrid theragnostic material that combines biological functionality with the physicochemical strengths of inorganic materials.

## 6. Conclusions

DB has served as an inspiration for the development of excellent biomaterials, offering unique structural advantages and eco-friendliness as strategic elements that enable diatoms to adapt to the environment. This natural material with a hierarchical porous structure and high biocompatibility is emerging as an innovative DDS platform that overcomes the limitations of existing synthetic carriers. In addition, leveraging their structural advantages, including surface functionalization capabilities, DB has garnered significant attention as a

versatile platform in the biosensing field. Therefore, DB demonstrates potential beyond simple drug carriers, positioning itself as a next-generation theragnostic biomaterial capable of simultaneously implementing diagnostic and therapeutic functions.

However, several critical limitations must be systematically addressed prior to the clinical expansion of DB. The primary challenge, achieving structural consistency, is that variations across different diatom species can significantly compromise the reproducibility of key performance parameters (e.g., including drug loading capacity, release kinetics, and biosensor signal consistency). This structural variability necessitates the development of standardized large-scale production processes and optimized purification protocols to ensure batch-to-batch uniformity. The comprehensive understanding of interaction mechanisms between DB surfaces and target molecules (e.g., drugs, proteins, DNA, and RNA) remains crucial for rational design and predictable performance. Equally important is the need for thorough toxicological evaluation, as current assessments of long-term *in vivo* behavior of DB and the safety profile of its degradation products are inadequate for clinical translation. Furthermore, concerns regarding the residual toxicity and immunogenicity of chemical reagents used during surface functionalization processes must be systematically investigated.

To address these multifaceted challenges, the development of reliable *in vivo* modeling systems is essential for accurately predicting DB performance in complex physiological environments, thereby bridging the gap between promising *in vitro* results and clinical reality. Overcoming these challenges will pave the way for DB to serve as a next-generation theragnostic platform in personalized precision medicine.

**Author Contributions:** D.Y. and M.L. contributed equally to this work. D.Y.: conceptualization, data curation, data analysis, writing the original draft, reviewing and editing; M.L.: conceptualization, data curation, data analysis, writing the original draft, reviewing and editing; Y.S.: data analysis, and reviewing and editing; J.Y.: reviewing and editing; E.J. and G.L.: data curation and data analysis; D.K.: data curation and editing; S.D.L.: review and editing; J.M.: conceptualization, review and editing; T.L.: conceptualization, data curation, writing the original draft, review and editing, and supervision. All authors have read and agreed to the published version of the manuscript.

**Funding:** This work was supported by the National Research Foundation of Korea (NRF) grant funded by the Korean government (MSIT) (RS-2024-00416117), by a study on the development of biomaterials for drug delivery using the biosilica of diatom (NNIBR20253104), and by Research Program funded by the National Research Council of Science & Technology (NST), (CRC22024-200) and by the Excellent Researcher Support Project of Kwangwoon University in 2025.

**Data Availability Statement:** Data will be available on request from the corresponding author.

**Conflicts of Interest:** The authors declare no conflicts of interest.

## References

1. Rozan, H.E.; Wu, G.; Zhou, Z.; Li, Q.; Sharaf, M.; Chen, X. The complex hydrogel based on diatom biosilica and hydroxybutyl chitosan for wound healing. *Colloids Surf. B Biointerfaces* **2022**, *216*, 112523. [CrossRef]
2. Dalgic, A.D.; Atila, D.; Tezcaner, A.; Gürses, S.; Keskin, D. Diatom silica frustules-doped fibers for controlled release of melatonin for bone regeneration. *Eur. Polym. J.* **2023**, *186*, 111858. [CrossRef]
3. Dolganyuk, V.; Belova, D.; Babich, O.; Prosekov, A.; Ivanova, S.; Katserov, D.; Patyukov, N.; Sukhikh, S. Microalgae: A Promising Source of Valuable Bioproducts. *Biomolecules* **2020**, *10*, 1153. [CrossRef] [PubMed]
4. Calijuri, M.L.; Silva, T.A.; Magalhães, I.B.; de Paula Pereira, A.S.A.; Marangon, B.B.; de Assis, L.R.; Lorentz, J.F. Bioproducts from Microalgae Biomass: Technology, Sustainability, Challenges and Opportunities. *Chemosphere* **2022**, *305*, 135508. [CrossRef] [PubMed]
5. Siddiki, S.Y.A.; Mofijur, M.; Kumar, P.S.; Ahmed, S.F.; Inayat, A.; Kusumo, F.; Badruddin, I.A.; Khan, T.M.Y.; Nghiem, L.D.; Ong, H.C. Microalgae Biomass as a Sustainable Source for Biofuel, Biochemical and Biobased Value-Added Products: An Integrated Biorefinery Concept. *Fuel* **2022**, *307*, 121782. [CrossRef]

6. Gautam, P.; Upadhyay, S.N.; Dubey, S.K. Bio-Methanol as a Renewable Fuel from Waste Biomass: Current Trends and Future Perspective. *Fuel* **2020**, *273*, 117783. [CrossRef]
7. Hussein, H.A.; Nazir, M.S.; Azra, N.; Qamar, Z.; Seeni, A.; Tengku Din, T.A.D.A.-A.; Abdullah, M.A. Novel Drug and Gene Delivery System and Imaging Agent Based on Marine Diatom Biosilica Nanoparticles. *Mar. Drugs* **2022**, *20*, 480. [CrossRef]
8. Kröger, N.; Poulsen, N. Diatoms—From Cell Wall Biogenesis to Nanotechnology. *Annu. Rev. Genet.* **2008**, *42*, 83–107. [CrossRef]
9. Maher, S.; Kumeria, T.; Aw, M.S.; Losic, D. Diatom Silica for Biomedical Applications: Recent Progress and Advances. *Adv. Heal. Mater.* **2018**, *7*, 1800552. [CrossRef]
10. Bak, M.; Molnár, F.; Rákosa, R.; Németh, Z.; Németh, R. Dimensional Stabilization of Wood by Microporous Silica Aerogel Using In-Situ Polymerization. *Wood Sci. Technol.* **2022**, *56*, 1353–1375. [CrossRef]
11. Terracciano, M.; De Stefano, L.; Rea, I. Diatoms Green Nanotechnology for Biosilica-Based Drug Delivery Systems. *Pharmaceutics* **2018**, *10*, 242. [CrossRef]
12. Sardo, A.; Orefice, I.; Balzano, S.; Barra, L.; Romano, G. Mini-Review: Potential of Diatom-Derived Silica for Biomedical Applications. *Appl. Sci.* **2021**, *11*, 4533. [CrossRef]
13. Delalat, B.; Sheppard, V.C.; Rasi Ghaemi, S.; Rao, S.; Prestidge, C.A.; McPhee, G.; Rogers, M.-L.; Donoghue, J.F.; Pillay, V.; Johns, T.G. Targeted Drug Delivery Using Genetically Engineered Diatom Biosilica. *Nat. Commun.* **2015**, *6*, 8791. [CrossRef]
14. Uthappa, U.T.; Brahmkhatri, V.; Sriram, G.; Jung, H.-Y.; Yu, J.; Kurkuri, N.; Aminabhavi, T.M.; Altalhi, T.; Neelgund, G.M.; Kurkuri, M.D. Nature Engineered Diatom Biosilica as Drug Delivery Systems. *J. Control. Release* **2018**, *281*, 70–83. [CrossRef]
15. Liu, Q.; Cai, W.; Zhen, T.; Ji, N.; Dai, L.; Xiong, L.; Sun, Q. Preparation of Debranched Starch Nanoparticles by Ionic Gelation for Encapsulation of Epigallocatechin Gallate. *Int. J. Biol. Macromol.* **2020**, *161*, 481–491. [CrossRef]
16. Zhu, H.; Zhu, E.; Xie, Y.; Liu, D.; Hu, Y.; Shi, Z.; Xiong, C.; Yang, Q. Hydrangea-like Nanocellulose Microspheres with High Dye Adsorption and Drug Encapsulation Prepared by Emulsion Method. *Carbohydr. Polym.* **2022**, *296*, 119947. [CrossRef]
17. Moretta, R.; De Stefano, L.; Terracciano, M.; Rea, I. Porous Silicon Optical Devices: Recent Advances in Biosensing Applications. *Sensors* **2021**, *21*, 1336. [CrossRef]
18. Liao, X.; Liu, J.; Yang, M.; Ma, H.; Yuan, B.; Huang, C.-H. Evaluation of Disinfection By-Product Formation Potential (DBPFP) during Chlorination of Two Algae Species—Blue-Green Microcystis Aeruginosa and Diatom Cyclotella Meneghiniana. *Sci. Total Environ.* **2015**, *532*, 540–547. [CrossRef] [PubMed]
19. Jin, P.; Agustí, S. Fast Adaptation of Tropical Diatoms to Increased Warming with Trade-Offs. *Sci. Rep.* **2018**, *8*, 17771. [CrossRef] [PubMed]
20. Cheng, L.-M.; Zhang, S.-F.; Xie, Z.-X.; Li, D.-X.; Lin, L.; Wang, M.-H.; Wang, D.-Z. Metabolic Adaptation of a Globally Important Diatom Following 700 Generations of Selection under a Warmer Temperature. *Environ. Sci. Technol.* **2022**, *56*, 5247–5255. [CrossRef] [PubMed]
21. Liang, Y.; Koester, J.A.; Liefer, J.D.; Irwin, A.J.; Finkel, Z.V. Molecular Mechanisms of Temperature Acclimation and Adaptation in Marine Diatoms. *ISME J.* **2019**, *13*, 2415–2425. [CrossRef]
22. Delasoie, J.; Zobi, F. Natural Diatom Biosilica as Microshuttles in Drug Delivery Systems. *Pharmaceutics* **2019**, *11*, 537. [CrossRef]
23. Mayzel, B.; Aram, L.; Varsano, N.; Wolf, S.G.; Gal, A. Structural Evidence for Extracellular Silica Formation by Diatoms. *Nat. Commun.* **2021**, *12*, 4639. [CrossRef]
24. Tesson, B.; Hildebrand, M. Dynamics of Silica Cell Wall Morphogenesis in the Diatom Cyclotella Cryptica: Substructure Formation and the Role of Microfilaments. *J. Struct. Biol.* **2010**, *169*, 62–74. [CrossRef]
25. Tesson, B.; Lerch, S.J.L.; Hildebrand, M. Characterization of a New Protein Family Associated with the Silica Deposition Vesicle Membrane Enables Genetic Manipulation of Diatom Silica. *Sci. Rep.* **2017**, *7*, 13457. [CrossRef]
26. Lechner, C.C.; Becker, C.F.W. Silaffins in Silica Biomineralization and Biomimetic Silica Precipitation. *Mar. Drugs* **2015**, *13*, 5297–5333. [CrossRef] [PubMed]
27. Trofimov, A.A.; Pawlicki, A.A.; Borodinov, N.; Mandal, S.; Mathews, T.J.; Hildebrand, M.; Ziatdinov, M.A.; Hausladen, K.A.; Urbanowicz, P.K.; Steed, C.A. Deep Data Analytics for Genetic Engineering of Diatoms Linking Genotype to Phenotype *via* Machine Learning. *NPJ Comput. Mater.* **2019**, *5*, 67. [CrossRef]
28. Görlich, S.; Pawolski, D.; Zlotnikov, I.; Kröger, N. Control of Biosilica Morphology and Mechanical Performance by the Conserved Diatom Gene Silicanin-1. *Commun. Biol.* **2019**, *2*, 245. [CrossRef]
29. Nemoto, M.; Iwaki, S.; Moriya, H.; Monden, Y.; Tamura, T.; Inagaki, K.; Mayama, S.; Obuse, K. Comparative Gene Analysis Focused on Silica Cell Wall Formation: Identification of Diatom-Specific SET Domain Protein Methyltransferases. *Mar. Biotechnol.* **2020**, *22*, 551–563. [CrossRef] [PubMed]
30. Hamm, C.E.; Merkel, R.; Springer, O.; Jurkojc, P.; Maier, C.; Prechtel, K.; Smetacek, V. Architecture and Material Properties of Diatom Shells Provide Effective Mechanical Protection. *Nature* **2003**, *421*, 841–843. [CrossRef]
31. De Tommasi, E.; Congestri, R.; Dardano, P.; De Luca, A.C.; Managò, S.; Rea, I.; De Stefano, M. UV-Shielding and Wavelength Conversion by Centric Diatom Nanopatterned Frustules. *Sci. Rep.* **2018**, *8*, 16285. [CrossRef]

32. Musenich, L.; Origo, D.; Gallina, F.; Buehler, M.J.; Libonati, F. Revealing Diatom-Inspired Materials Multifunctionality. *Adv. Funct. Mater.* **2025**, *35*, 2407148. [CrossRef]
33. Pawolski, D.; Heintze, C.; Mey, I.; Steinem, C.; Kröger, N. Reconstituting the Formation of Hierarchically Porous Silica Patterns Using Diatom Biomolecules. *J. Struct. Biol.* **2018**, *204*, 64–74. [CrossRef] [PubMed]
34. Kléparski, L.; Beaugrand, G.; Edwards, M.; Schmitt, F.G.; Kirby, R.R.; Breton, E.; Gevaert, F.; Maniez, E. Morphological Traits, Niche-Environment Interaction and Temporal Changes in Diatoms. *Prog. Oceanogr.* **2022**, *201*, 102747. [CrossRef]
35. Petrucciani, A.; Moretti, P.; Ortore, M.G.; Norici, A. Integrative Effects of Morphology, Silicification, and Light on Diatom Vertical Movements. *Front. Plant Sci.* **2023**, *14*, 1143998. [CrossRef]
36. Tréguer, P.; Bowler, C.; Moriceau, B.; Dutkiewicz, S.; Gehlen, M.; Aumont, O.; Bittner, L.; Dugdale, R.; Finkel, Z.; Iudicone, D. Influence of Diatom Diversity on the Ocean Biological Carbon Pump. *Nat. Geosci.* **2018**, *11*, 27–37. [CrossRef]
37. Ryderheim, F.; Grønning, J.; Kiørboe, T. Thicker Shells Reduce Copepod Grazing on Diatoms. *Limnol. Oceanogr. Lett.* **2022**, *7*, 435–442. [CrossRef]
38. Rajabi-Abhari, A.; Kim, J.N.; Lee, J.; Tabassian, R.; Mahato, M.; Youn, H.J.; Oh, I.K. Diatom bio-silica and cellu-lose nanofibril for bio-triboelectric nanogenerators and self-powered breath monitoring masks. *ACS Appl. Mater. Interfaces* **2020**, *13*, 219–232. [CrossRef]
39. Bondoc-Naumovitz, K.G.; Crosato, E.; Wan, K.Y. Functional Morphology of Gliding Motility in Benthic Diatoms. *Proc. Natl. Acad. Sci. USA* **2025**, *122*, e2426910122. [CrossRef]
40. Hansen, A.N.; Visser, A.W. The Seasonal Succession of Optimal Diatom Traits. *Limnol. Oceanogr.* **2019**, *64*, 1442–1457. [CrossRef]
41. Fan, J.; Li, F.; Hu, S.; Gao, K.; Xu, J. Larger Diatoms Are More Sensitive to Temperature Changes and Prone to Succumb to Warming Stress. *Limnol. Oceanogr.* **2023**, *68*, 2512–2528. [CrossRef]
42. Shimakawa, G.; Matsuda, Y. Extra $O_2$ evolution reveals an $O_2$-independent alternative electron sink in pho-tosynthesis of marine diatoms. *Photosynth. Res.* **2024**, *159*, 61–68. [CrossRef] [PubMed]
43. Smerilli, A.; Orefice, I.; Corato, F.; Gavalás Olea, A.; Ruban, A.V.; Brunet, C. Photoprotective and Antioxidant Responses to Light Spectrum and Intensity Variations in the Coastal Diatom Skeletonema Marinoi. *Environ. Microbiol.* **2017**, *19*, 611–627. [CrossRef]
44. Palanisamy, K.M.; Rahim, M.H.A.; Govindan, N.; Ramaraj, R.; Kuppusamy, P.; Maniam, G.P. Effect of Blue Light Intensity and Photoperiods on the Growth of Diatom Thalassiosira Pseudonana. *Bioresour Technol. Rep.* **2022**, *19*, 101152. [CrossRef]
45. Liu, M.; Hua, W.; Yu, C.; Zhang, S.; Li, W.; Li, C.; Peng, J.; Liu, R.; Liu, H.; Qu, J. Toxicity Mechanism of Microplastics on the Growth Traits and Metabolic Pathways of Vallisneria Natans under Different Light Environments. *Ecotoxicol. Environ. Saf.* **2025**, *291*, 117772. [CrossRef]
46. Muñoz-López, C.L.; Rivera-Rondón, C.A. Diatom Response to Environmental Gradients in the High Mountain Lakes of the Colombia's Eastern Range. *Aquat. Sci.* **2022**, *84*, 15. [CrossRef]
47. Fu, H.; Wang, P.; Wu, X.; Zhou, X.; Ji, G.; Shen, Y.; Gao, Y.; Li, Q.Q.; Liang, J. Distinct Genome-Wide Alternative Polyadenyl-ation during the Response to Silicon Availability in the Marine Diatom *Thalassiosira pseudonana*. *Plant J.* **2019**, *99*, 67–80. [CrossRef]
48. Naseema Rasheed, R.; Pourbakhtiar, A.; Mehdizadeh Allaf, M.; Baharlooeian, M.; Rafiei, N.; Alishah Aratboni, H.; Moro-nes-Ramirez, J.R.; Winck, F.V. Microalgal Co-Cultivation -Recent Methods, Trends in Omic-Studies, Applications, and Fu-ture Challenges. *Front. Bioeng. Biotechnol.* **2023**, *11*, 1193424. [CrossRef]
49. Schneider, R.J.; Roe, K.L.; Hansel, C.M.; Voelker, B.M. Species-Level Variability in Extracellular Production Rates of Reac-tive Oxygen Species by Diatoms. *Front. Chem.* **2016**, *4*, 5. [CrossRef] [PubMed]
50. Zepernick, B.N.; Gann, E.R.; Martin, R.M.; Pound, H.L.; Krausfeldt, L.E.; Chaffin, J.D.; Wilhelm, S.W. Elevated pH Conditions Associated with *Microcystis* spp. Blooms Decrease Viability of the Cultured Diatom *Fragilaria crotonensis* and Natural Diatoms in Lake Erie. *Front. Microbiol.* **2021**, *12*, 598736. [CrossRef] [PubMed]
51. Singh, P.K.; Bhattacharjya, R.; Marella, T.K.; Saxena, A.; Mishra, B.; Savio, S.; Tiwari, A. Production of Lipids and Proteins from Marine Diatoms under Changing pH and Silica. *Bioresour. Technol.* **2022**, *362*, 127766. [CrossRef]
52. Hervé, V.; Derr, J.; Douady, S.; Quinet, M.; Moisan, L.; Lopez, P.J. Multiparametric Analyses Reveal the pH-Dependence of Silicon Biomineralization in Diatoms. *PLoS ONE* **2012**, *7*, e46722. [CrossRef]
53. Petrou, K.; Baker, K.G.; Nielsen, D.A.; Hancock, A.M.; Schulz, K.G.; Davidson, A.T. Acidification Diminishes Diatom Silica Production in the Southern Ocean. *Nat. Clim. Change* **2019**, *9*, 781–786. [CrossRef]
54. Roubeix, V.; Lancelot, C. Effect of Salinity on Growth, Cell Size and Silicification of an Euryhaline Freshwater Diatom: Cyclotella meneghiniana Kütz. *Transit. Waters Bull.* **2008**, *1*, 1–38.
55. Hu, J.; Zheng, Y.; Yang, S.; Yang, L.; You, Q.; Wang, Q. Transcriptomic Analysis Reveals the Mechanism Underlying Salinity-Induced Morphological Changes in *Skeletonema subsalsum*. *Front. Microbiol.* **2024**, *15*, 1476738. [CrossRef]
56. Johnston, M.R.; Gascooke, J.R.; Ellis, A.V.; Leterme, S.C. Diatoms Response to Salinity Changes: Investigations Using Single Pulse and Cross Polarisation Magic Angle Spinning 29Si NMR Spectra. *Analyst* **2018**, *143*, 4930–4935. [CrossRef]
57. Javaheri, N.; Dries, R.; Burson, A.; Stal, L.J.; Sloot, P.M.A.; Kaandorp, J.A. Temperature Affects the Silicate Morphology in a Diatom. *Sci. Rep.* **2015**, *5*, 11652. [CrossRef]

58. Yi, Z.; Su, Y.; Cherek, P.; Nelson, D.R.; Lin, J.; Rolfsson, O.; Fu, W. Combined Artificial High-Silicate Medium and LED Illumination Promote Carotenoid Accumulation in the Marine Diatom *Phaeodactylum tricornutum*. Microb. *Cell. Fact.* **2019**, *18*, 209. [CrossRef] [PubMed]
59. Kim, J.; Fabris, M.; Baart, G.; Kim, M.K.; Goossens, A.; Vyverman, W.; Falkowski, P.G.; Lun, D.S. Flux Balance Analysis of Primary Metabolism in the Diatom *Phaeodactylum tricornutum*. *Plant J.* **2016**, *85*, 161–176. [CrossRef]
60. Wang, Y.; Zhang, D.; Cai, J.; Pan, J.; Chen, M.; Li, A.; Jiang, Y. Biosilica Structures Obtained from Nitzschia, Ditylum, Skeletonema, and Coscinodiscus Diatom by a Filtration-Aided Acid Cleaning Method. *Appl. Microbiol. Biotechnol.* **2012**, *95*, 1165–1178. [CrossRef]
61. Kröger, N.; Bergsdorf, C.; Sumper, M. A New Calcium Binding Glycoprotein Family Constitutes a Major Diatom Cell Wall Component. *EMBO J.* **1994**, *13*, 4676–4683. [CrossRef] [PubMed]
62. Gholami, P.; Khataee, A.; Bhatnagar, A. Environmentally Superior Cleaning of Diatom Frustules Using Sono-Fenton Process: Facile Fabrication of Nanoporous Silica with Homogeneous Morphology and Controlled Size. *Ultrason. Sonochem.* **2020**, *64*, 105044. [CrossRef]
63. Abate, R.; Song, S.; Patil, V.; Chen, C.; Liang, J.; Sun, L.; Li, X.; Huang, B.; Gao, Y. Enhancing the Production of a Marine Diatom (*Skeletonema costatum*) with Low-Frequency Ultrasonic Irradiation. *J. Appl. Phycol.* **2020**, *32*, 3711–3722. [CrossRef]
64. Annunziata, R.; Balestra, C.; Marotta, P.; Ruggiero, A.; Manfellotto, F.; Benvenuto, G.; Biffali, E.; Ferrante, M.I. An Optimised Method for Intact Nuclei Isolation from Diatoms. *Sci. Rep.* **2021**, *11*, 1681. [CrossRef]
65. Desai, A.R.; Maulvi, F.A.; Desai, D.M.; Shukla, M.R.; Ranch, K.M.; Vyas, B.A.; Shah, S.A.; Sandeman, S.; Shah, D.O. Multiple Drug Delivery from the Drug-Implants-Laden Silicone Contact Lens: Addressing the Issue of Burst Drug Release. *Mater. Sci. Eng. C.* **2020**, *112*, 110885. [CrossRef]
66. Seo, Y.; Woo, Y.; Oh, B.; Yoo, D.; Kwon, H.K.; Park, C.; Cho, H.Y.; Kim, H.S.; Lee, T. Microfluidic Fabrication of Oleosin-Coated Liposomes as Anticancer Drug Carriers with Enhanced Sustained Drug Release. *Materials* **2024**, *17*, 5550. [CrossRef]
67. Lim, H.; Seo, Y.; Kwon, D.; Kang, S.; Yu, J.; Park, H.; Lee, S.D.; Lee, T. Recent Progress in Diatom Biosilica: A Natural Nanoporous Silica Material as Sustained Release Carrier. *Pharmaceutics* **2023**, *15*, 2434. [CrossRef]
68. Dou, J.; Zhao, F.; Fan, W.; Chen, Z.; Guo, X. Preparation of Non-Spherical Vaterite $CaCO_3$ Particles by Flash Nano Precipitation Technique for Targeted and Extended Drug Delivery. *J. Drug Deliv. Sci. Technol.* **2020**, *57*, 101768. [CrossRef]
69. Wojtczak, I.; Brzozowska, W.; Bekissanova, Z.; Trykowski, G.; Rybczyński, P.; Ośmiałowski, B.; Sprynskyy, M. Diatom Biosilica Modified with Ce-Tb Mixed Oxide Twinning Nanoparticles and with Polyphases Quasi-Crystalline Tb Oxide Nanoparticles. *Colloids. Surf. A Physicochem. Eng. Asp.* **2025**, *704*, 135463. [CrossRef]
70. Saxena, A.; Dutta, A.; Kapoor, N.; Kumar, A.; Tiwari, A. Envisaging Marine Diatom *Thalassiosira weissflogii* as a "SMART" Drug Delivery System for Insoluble Drugs. *J. Drug Deliv. Sci. Technol.* **2022**, *68*, 102983. [CrossRef]
71. Kang, S.; Woo, Y.; Seo, Y.; Yoo, D.; Kwon, D.; Park, H.; Lee, S.D.; Yoo, H.Y.; Lee, T. A Descriptive Review on the Potential Use of Diatom Biosilica as a Powerful Functional Biomaterial: A Natural Drug Delivery System. *Pharmaceutics* **2024**, *16*, 1171. [CrossRef] [PubMed]
72. Li, M.; Wu, J.; Lin, D.; Yang, J.; Jiao, N.; Wang, Y.; Liu, L. A diatom-based biohybrid microrobot with a high drug-loading capacity and pH-sensitive drug release for target therapy. *Acta Biomater.* **2022**, *154*, 443–453. [CrossRef]
73. Siepmann, J.; Faisant, N.; Akiki, J.; Richard, J.; Benoit, J.P. Effect of the Size of Biodegradable Microparticles on Drug Release: Experiment and Theory. *J. Control. Release* **2004**, *96*, 123–134. [CrossRef]
74. Le, T.D.H. Hydrophobic and Hydrophilic Drug Loading Capacity of Micro Diatom Frustule from Diatomite. *J. Tech. Educ. Sci.* **2021**, *16*, 35–40. [CrossRef]
75. Ormerod, C. Opening a Window on Diffusion Polar Mixed Boundary Simulations for Diatom Controlled Release. Ph.D. Thesis, University of Wollongong, Wollongong, Australia, 2021.
76. Seo, Y.; Lim, H.; Park, H.; Yu, J.; An, J.; Yoo, H.Y.; Lee, T. Recent Progress of Lipid Nanoparticles-Based Lipophilic Drug Delivery: Focus on Surface Modifications. *Pharmaceutics* **2023**, *15*, 772. [CrossRef]
77. Ruan, S.; Zhou, Y.; Jiang, X.; Gao, H. Rethinking CRITID Procedure of Brain Targeting Drug Delivery: Circulation, Blood Brain Barrier Recognition, Intracellular Transport, Diseased Cell Targeting, Internalization, and Drug Release. *Adv. Sci.* **2021**, *8*, 2004025. [CrossRef]
78. Ulbrich, K.; Holá, K.; Šubr, V.; Bakandritsos, A.; Tuček, J.; Zbořil, R. Targeted Drug Delivery with Polymers and Magnetic Nanoparticles: Covalent and Noncovalent Approaches, Release Control, and Clinical Studies. *Chem. Rev.* **2016**, *116*, 5338–5431. [CrossRef]
79. Cicco, S.R.; Vona, D.; De Giglio, E.; Cometa, S.; Mattioli-Belmonte, M.; Palumbo, F.; Ragni, R.; Farinola, G.M. Chemically Modified Diatoms Biosilica for Bone Cell Growth with Combined Drug-Delivery and Antioxidant Properties. *Chempluschem* **2015**, *80*, 1104–1112. [CrossRef] [PubMed]
80. Gao, C.; Xu, J.; Xie, S.; Zhang, W.; Gong, D.; Peng, G.; Du, Z.; Rong, J.; Li, X.; Liang, C.; et al. Biotemplated Diatom Microrobots for Dual-Drug Delivery in Targeted Neuroblastoma Therapy. *ACS Appl. Mater. Interfaces* **2025**, *19*, 24807–24819. [CrossRef] [PubMed]

81. Story, B.D.; Park, S.; Roszak, K.; Shim, J.; Motta, M.; Ferneding, M.; Rudeen, K.M.; Blandino, A.; Ardon, M.; Le, S.; et al. Safety and Biocompatibility of a Novel Biodegradable Aflibercept-Drug Delivery System in Rhesus Macaques. *Drug Deliv.* **2025**, *32*, 2460671. [CrossRef]
82. Sprynskyy, M.; Szczyglewska, P.; Wojtczak, I.; Nowak, I.; Witkowski, A.; Buszewski, B.; Feliczak-Guzik, A.; Martins, M. Diatom Biosilica Doped with Palladium(II) Chloride Nanoparticles as New Efficient Photocatalysts for Methyl Orange Degradation. *Int. J. Mol. Sci. Artic.* **2021**, *22*, 6734. [CrossRef]
83. Miao, Y.; Feng, Y.; Bai, J.; Liu, Z.; Zhao, X. Optimized Mesoporous Silica Nanoparticle-Based Drug Delivery System with Removable Manganese Oxide Gatekeeper for Controlled Delivery of Doxorubicin. *J. Colloid Interface Sci.* **2021**, *592*, 227–236. [CrossRef] [PubMed]
84. Slowing, I.I.; Vivero-Escoto, J.L.; Wu, C.W.; Lin, V.S.Y. Mesoporous Silica Nanoparticles as Controlled Release Drug Delivery and Gene Transfection Carriers. *Adv. Drug Deliv. Rev.* **2008**, *60*, 1278–1288. [CrossRef]
85. Kempen, P.J.; Greasley, S.; Parker, K.A.; Campbell, J.L.; Chang, H.Y.; Jones, J.R.; Sinclair, R.; Gambhir, S.S.; Jokerst, J.V. Theranostic Mesoporous Silica Nanoparticles Biodegrade after Pro-Survival Drug Delivery and Ultrasound/Magnetic Resonance Imaging of Stem Cells. *Theranostics* **2015**, *5*, 631. [CrossRef]
86. Ashour, M.M.; Mabrouk, M.; Soliman, I.E.; Beherei, H.H.; Tohamy, K.M. Mesoporous Silica Nanoparticles Prepared by Different Methods for Biomedical Applications: Comparative Study. *IET Nanobiotechnol.* **2021**, *15*, 291–300. [CrossRef]
87. Putri, R.M.; Almunadya, N.S.; Amri, A.F.; Afnan, N.T.; Nurachman, Z.; Devianto, H.; Saputera, W.H. Structural Characterization of Polycrystalline Titania Nanoparticles on C. Striata Biosilica for Photocatalytic POME Degradation. *ACS Omega* **2022**, *7*, 44047–44056. [CrossRef] [PubMed]
88. Sun, Y.; Ma, K.; Kao, T.; Spoth, K.A.; Sai, H.; Zhang, D.; Kourkoutis, L.F.; Elser, V.; Wiesner, U. Formation Pathways of Mesoporous Silica Nanoparticles with Dodecagonal Tiling. *Nat. Commun.* **2017**, *8*, 252. [CrossRef] [PubMed]
89. Spitzmüller, L.; Nitschke, F.; Rudolph, B.; Berson, J.; Schimmel, T.; Kohl, T. Dissolution Control and Stability Improvement of Silica Nanoparticles in Aqueous Media. *J. Nanoparticle Res.* **2023**, *25*, 40. [CrossRef]
90. Sprynskyy, M.; Pomastowski, P.; Hornowska, M.; Król, A.; Rafińska, K.; Buszewski, B. Naturally Organic Functionalized 3D Biosilica from Diatom Microalgae. *Mater. Des.* **2017**, *132*, 22–29. [CrossRef]
91. Maher, S.; Alsawat, M.; Kumeria, T.; Fathalla, D.; Fetih, G.; Santos, A.; Habib, F.; Losic, D. Luminescent Silicon Diatom Replicas: Self-Reporting and Degradable Drug Carriers with Biologically Derived Shape for Sustained Delivery of Therapeutics. *Adv. Funct. Mater.* **2015**, *25*, 5107–5116. [CrossRef]
92. Heidegger, S.; Gößl, D.; Schmidt, A.; Niedermayer, S.; Argyo, C.; Endres, S.; Bourquin, C. Immune response to functionalized mesoporous silica nanoparticles for targeted drug delivery. *Nanoscale* **2016**, *8*, 938–948. [CrossRef]
93. Zhang, H.; Shahbazi, M.A.; Mäkilä, E.M.; da Silva, T.H.; Reis, R.L.; Salonen, J.J.; Santos, H.A. Diatom silica microparticles for sustained release and permeation enhancement following oral delivery of prednisone and mesalamine. *Biomaterials* **2013**, *34*, 9210–9219. [CrossRef]
94. Moodley, T.; Singh, M. Sterically Stabilised Polymeric Mesoporous Silica Nanoparticles Improve Doxorubicin Efficiency: Tailored Cancer Therapy. *Molecules* **2020**, *25*, 742. [CrossRef] [PubMed]
95. Ghasemi Shayan, R.; Jalaei, D.; Dobakhti, F. Modified diatom-based ocular suspension for sustained diclofenac sodium delivery: A novel drug carrier approach. *BMC Pharmacol. Toxicol.* **2025**, *26*, 77.
96. Kolimi, P.; Narala, S.; Youssef, A.A.A.; Nyavanandi, D.; Dudhipala, N. A systemic review on development of mesoporous nanoparticles as a vehicle for transdermal drug delivery. *Nanotheranostics* **2023**, *7*, 70. [CrossRef]
97. An, J.; Park, H.; Ju, M.; Woo, Y.; Seo, Y.; Min, J.; Lee, T. An Updated Review on the Development of a Nanomaterial-Based Field-Effect Transistor-Type Biosensors to Detect Exosomes for Cancer Diagnosis. *Talanta* **2024**, *279*, 126604. [CrossRef]
98. Li, M.; Liu, D.; Wang, S.; Guo, H.; Losic, D.; Deng, L.; Wu, S.; Yuan, P. Efficient Removal of $Cd^{2+}$ by Diatom Frustules Self-Modified in Situ with Intercellular Organic Components. *Environ. Pollut.* **2023**, *319*, 121005. [CrossRef]
99. Kumari, E.; Görlich, S.; Poulsen, N.; Kröger, N. Genetically Programmed Regioselective Immobilization of Enzymes in Biosilica Microparticles. *Adv. Funct. Mater.* **2020**, *30*, 2000442. [CrossRef]
100. Wu, Y.; Wang, C.W.; Wang, D.; Wei, N. A Whole-Cell Biosensor for Point-of-Care Detection of Waterborne Bacterial Pathogens. *ACS Synth. Biol.* **2021**, *10*, 333–344. [CrossRef]
101. Messaabi, A.; Merindol, N.; Bohnenblust, L.; Fantino, E.; Meddeb-Mouelhi, F.; Desgagné-Penix, I. *In Vivo* Thrombin Activity in the Diatom *Phaeodactylum tricornutum*: Biotechnological Insights. *Appl. Microbiol. Biotechnol.* **2024**, *108*, 481. [CrossRef] [PubMed]
102. Yu, L.; Peng, Y.; Sheng, M.; Wang, Q.; Huang, J.; Yang, X. Sensitive and Amplification-Free Electrochemiluminescence Biosensor for HPV-16 Detection Based on CRISPR/Cas12a and DNA Tetrahedron Nanostructures. *ACS Sens.* **2023**, *8*, 2852–2858. [CrossRef] [PubMed]
103. Liu, Z.; Huang, Q.; Yan, Y.; Yao, J.; Zhong, F.; Xie, S.; Zhang, M.; Zhang, H.; Jin, M.; Shui, L. A Multi-Unit Integrated Electrochemical Biosensor Array for Synergistic Signal Enhancing Carbohydrate Antigen 125 Detection. *Sens. Actuators B Chem.* **2023**, *393*, 134224. [CrossRef]

104. Cvjetinovic, J.; Merdalimova, A.A.; Kirsanova, M.A.; Somov, P.A.; Nozdriukhin, D.V.; Salimon, A.I.; Korsunsky, A.M.; Gorin, D.A. A SERS Platform Based on Diatomite Modified by Gold Nanoparticles Using a Combination of Layer-by-Layer Assembly and a Freezing-Induced Loading Method. *Phys. Chem. Chem. Phys.* **2022**, *24*, 8901–8912. [CrossRef]
105. Saridag, A.M.; Karagoz, I.D.; Wachsmann-Hogiu, S.; Kahraman, M. Diatomite-Based, Flexible SERS Immunosensor Platform for Rapid, Specific, and Sensitive Detection of Circulating Cancer-Specific Protein Biomarkers in Serum Using Raman Probes. *ACS Appl. Bio Mater.* **2024**, *7*, 1878–1887. [CrossRef]
106. Tabassum, R.; Sarkar, P.P.; Jalal, A.H.; Ashraf, A.; Islam, N. Laser-induced electrochemical biosensor modified with graphene-based ink for label-free detection of alpha-fetoprotein and 17β-estradiol. *Polymers* **2024**, *16*, 2069. [CrossRef]
107. Li, P.; Li, T.; Feng, X.; Liu, D.; Zhong, Q.; Fang, X.; Wang, L. A micro-carbon nanotube transistor for ultra-sensitive, label-free, and rapid detection of Staphylococcal enterotoxin C in food. *J. Hazard. Mater.* **2023**, *449*, 131033. [CrossRef]
108. Wang, H.; Cai, J.; Wang, T.; Yan, R.; Shen, M.; Zhang, J.; Wang, J. Functionalized gold nanoparticle enhanced nanorod hyperbolic metamaterial biosensor for highly sensitive detection of carcinoembryonic antigen. *Biosens. Bioelectron.* **2024**, *257*, 116295. [CrossRef]
109. Beck, F.; Horn, C.; Baeumner, A.J. Dry-reagent microfluidic biosensor for simple detection of NT-proBNP *via* Ag nanoparticles. *Anal. Chim. Acta* **2022**, *1191*, 339375. [CrossRef]
110. Wang, W.; Ma, Z.; Shao, Q.; Wang, J.; Wu, L.; Huang, X.; He, L. Multi-MXene assisted large-scale manufacturing of electrochemical biosensors based on enzyme-nanoflower enhanced electrodes for the detection of $H_2O_2$ secreted from live cancer cells. *Nanoscale* **2024**, *16*, 12586–12598. [CrossRef] [PubMed]
111. Park, H.; Kwon, N.; Park, G.; Jang, M.; Kwon, Y.; Yoon, Y.; An, J.; Min, J.; Lee, T. Fast-Response Electrochemical Biosensor Based on a Truncated Aptamer and MXene Heterolayer for West Nile Virus Detection in Human Serum. *Bioelectrochemistry* **2023**, *154*, 108540. [CrossRef] [PubMed]
112. Kwon, Y.; Lee, M.; Kaushik, N.K.; Yoo, H.Y.; Park, C.; Lee, M.H.; Lee, T. Electrochemical Cell-SELEX Monitoring and Its Application to Electrochemical Aptasensor for Colorectal Cancer Detection. *Chem. Eng. J.* **2025**, *506*, 159935. [CrossRef]
113. Kim, G.; Li, Y.G.; Seo, Y.; Baek, C.; Choi, J.H.; Park, H.; An, J.; Lee, M.; Noh, S.; Min, J.; et al. Fabrication of Graphene Oxide-Based Pretreatment Filter and Electrochemical-CRISPR Biosensor for the Field-Ready Cyanobacteria Monitoring System. *Biosens. Bioelectron.* **2023**, *237*, 115474. [CrossRef]
114. dos Reis, G.S.; Dotto, G.L.; Vieillard, J.; Oliveira, M.L.S.; Lütke, S.F.; Silva, L.F.O.; Lima, É.C.; Salau, N.P.G.; Lassi, U. Uptake the Rare Earth Elements Nd, Ce, and La by a Commercial Diatomite: Kinetics, Equilibrium, Thermodynamic and Adsorption Mechanism. *J. Mol. Liq.* **2023**, *389*, 122862. [CrossRef]
115. Zakariah, E.I.; Ariffin, E.Y.; Nokarajoo, D.; Mohamed Akbar, M.A.; Lee, Y.H.; Hasbullah, S.A. Highly Sensitive of an Electrochemical DNA Biosensor Detection towards Toxic Dinoflagellates *Alexandrium minutum* (*A. minutum*). *Microchem. J.* **2024**, *199*, 109997. [CrossRef]
116. Silva, M.; Briceño, S.; Vizuete, K.; Debut, A.; González, G. Structural and Electrochemical Characterization of Diatomite with Lignin, Glucose, Activated Carbon and Magnetic Nanoparticles. *Carbon Trends* **2025**, *19*, 100492. [CrossRef]
117. Gao, C.; Zhang, W.; Gong, D.; Liang, C.; Su, Y.; Peng, G.; Deng, X.; Xu, W.; Cai, J. Biotemplated Janus Magnetic Microrobots Based on Diatomite for Highly Efficient Detection of Salmonella. *ACS Appl. Mater. Interfaces* **2024**, *16*, 49030–49040. [CrossRef]
118. Yoon, J.; Kwon, N.; Lee, Y.; Kim, S.; Lee, T.; Choi, J.W. Nanotechnology-Based Wearable Electrochemical Biosensor for Disease Diagnosis. *ACS Sens.* **2025**, *10*, 1675–1689. [CrossRef] [PubMed]
119. Ghobara, M.; Oschatz, C.; Fratzl, P.; Reissig, L. Numerical Analysis of the Light Modulation by the Frustule of *Gomphonema parvulum*: The Role of Integrated Optical Components. *Nanomaterials* **2023**, *13*, 113. [CrossRef]
120. De Tommasi, E.; Rea, I.; Ferrara, M.A.; De Stefano, L.; De Stefano, M.; Al-Handal, A.Y.; Stamenković, M.; Wulff, A. Multiple-Pathways Light Modulation in Pleurosigma Strigosum Bi-Raphid Diatom. *Sci. Rep.* **2024**, *14*, 6476. [CrossRef]
121. León-Valencia, A.; Briceño, S.; Reinoso, C.; Vizuete, K.; Debut, A.; Caetano, M.; González, G. Photochemical Reduction of Silver Nanoparticles on Diatoms. *Mar. Drugs* **2023**, *21*, 185. [CrossRef]
122. Ide, Y.; Matsukawa, Y. Fundamental Research on Functionalization of Diatomite Using DNA-Coated Single-Walled Carbon Nanotubes. *J. Photochem. Photobiol. A Chem.* **2024**, *452*, 115550. [CrossRef]
123. Chen, T.; Wu, F.; Li, Y.; Rozan, H.E.; Chen, X.; Feng, C. Gold nanoparticle-functionalized diatom biosilica as label-free biosensor for biomolecule detection. *Front. Bioeng. Biotechnol.* **2022**, *10*, 894636. [CrossRef] [PubMed]
124. Kamińska, A.; Sprynskyy, M.; Winkler, K.; Szymborski, T. Ultrasensitive SERS immunoassay based on diatom biosilica for detection of interleukins in blood plasma. *Anal. Bioanal. Chem.* **2017**, *409*, 6337–6347. [CrossRef] [PubMed]
125. Shapturenka, P.; Isaac Zakaria, N.; Birkholz, F.; Gordon, M.J. Extending the Diatom's Color Palette: Non-Iridescent, Disorder-Mediated Coloration in Marine Diatom-Inspired Nanomembranes. *Opt. Express* **2023**, *31*, 21658–21671. [CrossRef] [PubMed]
126. Wang, Y.Q.; Cao, C.; Ying, Y.L.; Li, S.; Wang, M.B.; Huang, J.; Long, Y.T. Rationally Designed Sensing Selectivity and Sensitivity of an Aerolysin Nanopore *via* Site-Directed Mutagenesis. *ACS Sens.* **2018**, *3*, 779–783. [CrossRef] [PubMed]

127. Zobi, F. Diatom Biosilica in Targeted Drug Delivery and Biosensing Applications: Recent Studies. *Micro* **2022**, *2*, 342–360. [CrossRef]
128. Park, S.; Cho, E.; Chueng, S.T.D.; Yoon, J.S.; Lee, T.; Lee, J.H. Aptameric Fluorescent Biosensors for Liver Cancer Diagnosis. *Biosensors* **2023**, *13*, 617. [CrossRef]
129. Broccoli, A.; Carnevale, L.; Mayorga González, R.; Dorresteijn, J.M.; Weckhuysen, B.M.; Olthuis, W.; Odijk, M.; Meirer, F. Accessibility Study of Porous Materials at the Single-Particle Level as Evaluated within a Microfluidic Chip with Fluorescence Microscopy. *Chem. Catal.* **2023**, *3*, 100791. [CrossRef]
130. Wang, Y.; Cai, J.; Jiang, Y.; Jiang, X.; Zhang, D. Preparation of Biosilica Structures from Frustules of Diatoms and Their Applications: Current State and Perspectives. *Appl. Microbiol. Biotechnol.* **2013**, *97*, 453–460. [CrossRef]
131. Gilic, M.; Ghobara, M.; Reissig, L. Tuning SERS Signal *via* Substrate Structuring: Valves of Different Diatom Species with Ultrathin Gold Coating. *Nanomaterials* **2023**, *13*, 1594. [CrossRef]
132. Mu, Y.; Zhang, M.; Sun, H.; Zhang, Q.; Chen, X.; Feng, C. Composite Diatom Fluorescent Sensor Substrate Enriched with CdSe/ZnS Quantum Dots on the Surface by Biofabrication. *Colloids Surf. B Biointerfaces* **2025**, *246*, 114396. [CrossRef]
133. Wang, Z.; Gong, D.; Cai, J. Diatom Frustule Array for Flow-through Enhancement of Fluorescent Signal in a Microfluidic Chip. *Micromachines* **2021**, *12*, 1017. [CrossRef]
134. Sun, X.; Zhang, M.; Liu, J.; Hui, G.; Chen, X.; Feng, C. The art of exploring diatom biosilica biomaterials: From biofabrication perspective. *Adv. Sci.* **2024**, *11*, 2304695. [CrossRef]
135. Esfandyari, J.; Shojaedin-Givi, B.; Hashemzadeh, H.; Mozafari-Nia, M.; Vaezi, Z.; Naderi-Manesh, H. Capture and Detection of Rare Cancer Cells in Blood by Intrinsic Fluorescence of a Novel Functionalized Diatom. *Photodiagnosis Photodyn. Ther.* **2020**, *30*, 101753. [CrossRef] [PubMed]
136. Wang, J.K.; Seibert, M. Prospects for Commercial Production of Diatoms. *Biotechnol. Biofuels* **2017**, *10*, 16. [CrossRef] [PubMed]
137. Wu, Y.; Wang, L.; Zhao, X.; Hou, S.; Guo, B.; Ma, P.X. Self-Healing Supramolecular Bioelastomers with Shape Memory Property as a Multifunctional Platform for Biomedical Applications *via* Modular Assembly. *Biomaterials* **2016**, *104*, 18–31. [CrossRef] [PubMed]
138. Nakielski, P.; Pawłowska, S.; Rinoldi, C.; Ziai, Y.; De Sio, L.; Urbanek, O.; Zembrzycki, K.; Pruchniewski, M.; Lanzi, M.; Salatelli, E.; et al. Multifunctional Platform Based on Electrospun Nanofibers and Plasmonic Hydrogel: A Smart Nanostructured Pillow for Near-Infrared Light-Driven Biomedical Applications. *ACS Appl. Mater. Interfaces* **2020**, *12*, 54328–54342. [CrossRef]
139. Park, G.; Kang, S.; Kwon, Y.; An, J.; Park, H.; Lee, M.H.; Lee, T. Electrical Capacitance-Based Cancer Cell Viability Monitoring Device for Accelerated Drug Development. *Sens. Actuators B Chem.* **2024**, *409*, 135566. [CrossRef]
140. Lee, D.E.; Koo, H.; Sun, I.C.; Ryu, J.H.; Kim, K.; Kwon, I.C. Multifunctional Nanoparticles for Multimodal Imaging and Theragnosis. *Chem. Soc. Rev.* **2012**, *41*, 2656–2672. [CrossRef]
141. Aboagye, E.O.; Barwick, T.D.; Haberkorn, U. Radiotheranostics in Oncology: Making Precision Medicine Possible. *CA Cancer J. Clin.* **2023**, *73*, 255–274. [CrossRef]
142. Medeiros Borsagli, F.G.L.; de Souza, A.J.M.; Paiva, A.E. Ecofriendly Multifunctional Thiolated Carboxymethyl Chitosan-Based 3D Scaffolds with Luminescent Properties for Skin Repair and Theragnostic of Tissue Regeneration. *Int. J. Biol. Macromol.* **2020**, *165*, 3051–3064. [CrossRef]
143. Conklin, B.; Conley, B.M.; Hou, Y.; Chen, M.; Lee, K.B. Advanced Theragnostics for the Central Nervous System (CNS) and Neurological Disorders Using Functional Inorganic Nanomaterials. *Adv. Drug Deliv. Rev.* **2023**, *192*, 1114636. [CrossRef] [PubMed]
144. Yi, K.; Rong, Y.; Huang, L.; Tang, X.; Zhang, Q.; Wang, W.; Wu, J.; Wang, F. Aptamer-Exosomes for Tumor Theranostics. *ACS Sens.* **2021**, *6*, 1418–1429. [CrossRef]
145. Sze, J.Y.Y.; Ivanov, A.P.; Cass, A.E.G.; Edel, J.B. Single Molecule Multiplexed Nanopore Protein Screening in Human Serum Using Aptamer Modified DNA Carriers. *Nat. Commun.* **2017**, *8*, 1552. [CrossRef]
146. Alshaer, W.; Hillaireau, H.; Vergnaud, J.; Ismail, S.; Fattal, E. Functionalizing Liposomes with Anti-CD44 Aptamer for Selective Targeting of Cancer Cells. *Bioconjug. Chem.* **2015**, *26*, 1307–1313. [CrossRef]
147. Kim, D.M.; Kim, M.; Park, H.B.; Kim, K.S.; Kim, D.E. Anti-MUC1/CD44 Dual-Aptamer-Conjugated Liposomes for Cotargeting Breast Cancer Cells and Cancer Stem Cells. *ACS Appl. Bio. Mater.* **2019**, *2*, 4622–4633. [CrossRef] [PubMed]
148. Hess, K.L.; Medintz, I.L.; Jewell, C.M. Designing Inorganic Nanomaterials for Vaccines and Immunotherapies. *Nano Today* **2019**, *27*, 73–98. [CrossRef] [PubMed]
149. Wang, X.; Zhong, X.; Li, J.; Liu, Z.; Cheng, L. Inorganic Nanomaterials with Rapid Clearance for Biomedical Applications. *Chem. Soc. Rev.* **2021**, *50*, 8669–8742. [CrossRef]
150. Frickenstein, A.N.; Hagood, J.M.; Britten, C.N.; Abbott, B.S.; McNally, M.W.; Vopat, C.A.; Patterson, E.G.; Maccuaig, W.M.; Jain, A.; Walters, K.B.; et al. Mesoporous Silica Nanoparticles: Properties and Strategies for Enhancing Clinical Effect. *Pharmaceutics* **2021**, *13*, 570. [CrossRef]
151. Živojević, K.; Mladenović, M.; Djisalov, M.; Mundzic, M.; Ruiz-Hernandez, E.; Gadjanski, I.; Knežević, N. Advanced Mesoporous Silica Nanocarriers in Cancer Theranostics and Gene Editing Applications. *J. Control. Release* **2021**, *337*, 193–211. [CrossRef]

152. Zhou, S.; Zhong, Q.; Wang, Y.; Hu, P.; Zhong, W.; Huang, C.B.; Yu, Z.Q.; Ding, C.D.; Liu, H.; Fu, J. Chemically Engineered Mesoporous Silica Nanoparticles-Based Intelligent Delivery Systems for Theranostic Applications in Multiple Cancerous/Non-Cancerous Diseases. *Coord. Chem. Rev.* **2022**, *452*, 214309. [CrossRef]
153. Xu, B.; Li, S.; Shi, R.; Liu, H. Multifunctional Mesoporous Silica Nanoparticles for Biomedical Applications. *Signal Transduct. Target. Ther.* **2023**, *8*, 435. [CrossRef]
154. Wells, C.M.; Harris, M.; Choi, L.; Murali, V.P.; Guerra, F.D.; Jennings, J.A. Stimuli-Responsive Drug Release from Smart Polymers. *J. Funct. Biomater.* **2019**, *10*, 34. [CrossRef]
155. Kashin, A.D.; Sedelnikova, M.B.; Chebodaeva, V.V.; Uvarkin, P.V.; Luginin, N.A.; Dvilis, E.S.; Bakina, O.V. Diatomite-based ceramic biocoating for magnesium implants. *Ceram. Int.* **2022**, *48*, 28059–28071. [CrossRef]
156. Han, Y.; Du, L.; Wu, J.; Zhang, H.; Yang, G.; Zheng, Y.; Wu, C. Diatomaceous cross-species constructs for tendon-to-bone regeneration. *Mater. Today* **2025**, *83*, 64–84. [CrossRef]
157. Brzozowska, W.; Sprynskyy, M.; Wojtczak, I.; Dąbek, P.; Markuszewski, M.J.; Witkowski, A.; Buszewski, B. Metabolically Doping of 3D Diatomaceous Biosilica with Titanium. *Materials* **2022**, *15*, 5210. [CrossRef]
158. Tramontano, C.; Chianese, G.; Terracciano, M.; de Stefano, L.; Rea, I. Nanostructured Biosilica of Diatoms: From Water World to Biomedical Applications. *Appl. Sci.* **2020**, *10*, 6811. [CrossRef]
159. Mu, Y.; Fu, Y.; Li, J.; Shao, K.; Pang, J.; Su, C.; Cai, Y.; Sun, X.; Cong, X.; Chen, X.; et al. Thrombin Immobilized Polydopamine-Diatom Biosilica for Effective Hemorrhage Control. *Biomater. Sci.* **2021**, *9*, 4952–4967. [CrossRef] [PubMed]
160. Hussein, H.A.; Abdullah, M.A. Anticancer Compounds Derived from Marine Diatoms. *Mar. Drugs* **2020**, *18*, 356. [CrossRef]


**Disclaimer/Publisher's Note:** The statements, opinions and data contained in all publications are solely those of the individual author(s) and contributor(s) and not of MDPI and/or the editor(s). MDPI and/or the editor(s) disclaim responsibility for any injury to people or property resulting from any ideas, methods, instructions or products referred to in the content.